

Impact of nonlinear energy transfer on the wave field in Pacific hindcast experiments

Hitoshi Tamura,¹ Takuji Waseda,^{1,2} and Yasumasa Miyazawa¹

Received 30 November 2009; revised 20 July 2010; accepted 25 August 2010; published 16 December 2010.

[1] We investigated the impact of nonlinear energy transfer (S_{nl}) on wave fields by performing hindcast experiments for the Pacific Ocean. Specifically, we evaluated model performance using SRIAM, which was developed to accurately reproduce S_{nl} with lower computational cost than more rigorous algorithms. The model results were compared to in situ wave parameters as well as results from another model employing the widely used discrete interaction approximation method (DIA). Comparison of the model results with buoy observations revealed a negligible difference between SRIAM and DIA for significant wave heights. However, the difference for the peak period was quite pronounced, especially around the tropical Pacific, where a persistent bias in peak frequency was improved by using SRIAM. This study also highlights the impact of source terms on spectral shape under a realistic model setting. Detailed analysis of spectral shape indicated that SRIAM can quantitatively capture the overshoot phenomena around the spectral peak during wave growth. In addition, S_{nl} played a major role in maintaining the equilibrium range; it reacted to changes in the net external sources to cancel out the total source term. These results show that the magnitude of high-frequency dissipation controls the spectral tail exponent and that the balanced net external source is responsible for the reproduction of the f^{-4} power law behavior in the equilibrium range.

Citation: Tamura, H., T. Waseda, and Y. Miyazawa (2010), Impact of nonlinear energy transfer on the wave field in Pacific hindcast experiments, *J. Geophys. Res.*, 115, C12036, doi:10.1029/2009JC006014.

1. Introduction

[2] Global and regional wave forecasting using third-generation wave models is now routinely conducted thanks to advances in numerical weather prediction, satellite scatterometer data, and computational resources. Wave-forecasting systems have also improved as a result of recent progress in numerical modeling, such as the implementation of data assimilation, introduction of higher-order numerical schemes, and coupling with atmosphere and ocean models. Remarkable model performance has been attained in estimating wave parameters such as the significant wave height (H_s) and the peak period (T_p) derived from the wave spectrum [Bidlot *et al.*, 2007].

[3] At present, nonlinear energy transfer (S_{nl}) is widely considered one of the most important factors controlling the evolution of wave spectra, such as the downshifting of the spectral peak, self-stabilization of the spectral form during wave growth, and frequency dependence of the directional spreading function [Young and Van Vledder, 1993]. These properties induce some interesting and important characteristics of the wave spectrum known as the overshoot phe-

nomenon [Barnett and Wilkerson, 1967; Mitsuyasu, 1968, 1969; Hasselmann *et al.*, 1973] and the power law of the equilibrium range [e.g., Zakharov and Filonenko, 1966; Toba, 1973; Kitaigorodskii, 1983; Phillips, 1985]. In addition, many studies have indicated the importance of S_{nl} in the formation of the bimodal directional distribution of the wave spectrum in the higher-frequency region [e.g., Banner and Young, 1994; Long and Resio, 2007]. It is crucial to use an accurate and sophisticated numerical scheme for S_{nl} to improve third-generation wave models [Van Vledder, 2006b] and to expand potential applicability to more general situations, such as slanting fetch wave growth [Arduin *et al.*, 2007].

[4] In operational wave forecasting and hindcasting, the choice of an S_{nl} algorithm is rather limited compared to other source terms (wind input, S_{in} ; white-capping, S_{ds}). S_{nl} is the only term that has an exact expression in terms of the Boltzmann integral [Hasselmann, 1962]. However, accurate evaluation of S_{nl} requires huge computational costs because there are infinite numbers of four-wave configurations that satisfy the resonant conditions. Consequently, no rigorous method of S_{nl} evaluation has been applied to operational wave forecasting. At present, the discrete interaction approximation method (DIA) proposed by Hasselmann *et al.* [1985] is most commonly used to estimate S_{nl} . In the DIA approach, the infinite number of configurations is substituted with a single combination of resonant quadruplets. The computational costs of DIA are considerably lower; however, this method

¹Research Institute for Global Change, Japan Agency for Marine-Earth Science and Technology, Yokohama, Kanagawa, Japan.

²Department of Ocean Technology Policy and Environment, Graduate School of Frontier Sciences, University of Tokyo, Chiba, Japan.

does not properly represent the nonlinear transfer rate compared to the exact solutions for the Boltzmann integral [e.g., Hasselmann *et al.*, 1985; Tolman, 2004]. Therefore, third-generation wave forecasting systems will not improve as long as DIA is used [Van Vledder *et al.*, 2000]. Ardhuin *et al.* [2007] reported that replacing DIA with an exact S_{nl} method (the WRT method; Van Vledder, [2006a]) caused the spectral shape to differ more from observations. They concluded that this result was due to the lack of retuning of the S_{in} and S_{ds} source terms, which were tuned for DIA in the WAM.

[5] Recent advances in computational resources have now made it possible to apply more expensive S_{nl} schemes to the operational wave model. New S_{nl} schemes have been developed that extend the original DIA [e.g., Van Vledder, 2001; Tolman, 2004], and other methods have also been proposed [Komatsu, 1996; Tolman *et al.*, 2005; Resio and Perrie, 2008]. Komatsu [1996] developed the simplified RIAM method (SRIAM), which utilizes 20 resonance configurations that retain the general properties of the S_{nl} kernel function. Komatsu [1996] showed that SRIAM performed favorably compared to the rigorous RIAM method [Komatsu and Masuda, 1996] for duration-limited wave growth after an abrupt change in wind direction and the evolution of perturbed-equilibrium spectra. Tamura *et al.* [2008] also assessed the performance of SRIAM by applying it to more complex situations, such as wave propagation against a shear current. They found that the use of SRIAM as the numerical scheme for S_{nl} modified the spectral shape. For example, the spectral shapes estimated by RIAM and SRIAM were much narrower in frequency and directional space than those estimated by DIA, where a peculiar trimodal directional distribution appeared around the low-frequency region. In addition, the self-stabilization effect of S_{nl} was demonstrated in a realistic wave simulation forced by reanalysis products of wind and ocean currents. They concluded that a realistic representation of the S_{nl} term is crucial for accurate evaluation of spectral modulation.

[6] The present paper investigates model performance in more detail using SRIAM based on hindcast experiments. We are interested in how sensitive wave parameters such as the H_s and the frequency peak (f_p) are to the numerical schemes of S_{nl} under realistic conditions. Specifically, the present study was motivated by a desire to elucidate whether accurate S_{nl} schemes improve the model representation of spectral shape in terms of freak wave prediction. Recent studies [e.g., Onorato *et al.*, 2002; Janssen, 2003; Gramstad and Trulsen, 2007; Waseda *et al.*, 2009a, 2009b] have suggested that owing to nonlinear focusing, the probability of a freak wave occurring increases as the wave spectrum narrows in the frequency and directional domains. Therefore, it is crucial to estimate the spectral shape as accurately as possible, which should lead to an improved prediction of abnormal waves. Whereas numerous studies have noted the importance of accurate evaluation of nonlinear transfer in operational wave forecasting, few have attempted to investigate its impact in a realistic situation. The applicability and model performance of SRIAM are investigated here by comparing in situ data provided by the National Oceanic and Atmospheric Administration/National Data Buoy Center (NOAA/NDBC) and computational results by DIA for hindcast simulations. We are also interested in the formation mechanism of the wave spectrum in terms of the source balance, as has been

discussed extensively by many researchers. We investigate the role of S_{nl} in the source balance in conjunction with the parameterization of the S_{ds} term.

[7] The remainder of this paper is arranged as follows. Section 2 describes the model configuration and design of the hindcast experiment. In section 3, we examine the basic properties of SRIAM for wave parameters by comparing in situ data and computational results obtained using DIA. In section 4, the effect of nonlinear energy transfer on the spectral shape is investigated in detail, mainly using SRIAM; this section also discusses the role of other source terms. Finally, a summary and discussion are given in section 5.

2. Model Configurations and Hindcast Experiments

2.1. Wave Model

[8] Wave hindcast was conducted based on WAVEWATCH-III version 2.22 [WW3; Tolman, 2002] with SRIAM as S_{nl} to investigate the impact of the improved S_{nl} scheme on the wave parameters and to test the applicability of SRIAM under realistic conditions. Numerical simulation using DIA (i.e., the default setting of WW3) was also conducted as a reference. In this study, we compared the model results of WW3/SRIAM and WW3/DIA. For all calculations, we used the same source functions of S_{in} and S_{ds} and a fixed spectral resolution because our goal was to investigate the impact of S_{nl} on the hindcast experiments. Tolman and Chalikov's [1996] (hereafter TC96) wave-growth and wave-decay source terms were used, and the surface wind speed at 10 m elevation was modified to consider the instability of the atmospheric boundary layer (the "effective" wind speed; Tolman, 2002). The spectral space was discretized using 25 frequencies ranging from 0.042 to 0.414 (relative frequency of 10%, $f_{m+1} = 1.1f_m$, where f is the intrinsic frequency and m is a discrete grid counter) with 36 directions ($\Delta\theta = 10^\circ$). Typical operational wave models, including WW3, apply a parametric spectral tail beyond a cutoff frequency for two primary reasons: to reduce computational costs and to impose an equilibrium spectrum with empirical law. In WW3, a parametric tail assuming the f^{-5} power law was patched to the frequency range from $2.5f_p$ to the end of the prognostic model frequency (here, 0.414 Hz) when $2.5f_p$ is lower than the highest frequency. Because one of our objectives was to investigate the spectral shape in the high-frequency region, we did not use the parametric spectral tail for either model setting (WW3/SRIAM or WW3/DIA). That is, the energy density in the prognostic frequency region was fully controlled by the source and propagation terms. However, the spectral tail is necessary for computing S_{nl} when the highest frequency corresponding to the four resonant waves is larger than the highest discrete model frequency. Therefore, we assumed an f^{-5} spectral tail outside the model frequency range (greater than 0.414 Hz), as used in the default WW3 settings. For spatial propagation of the wave spectrum, we used the default third-order advection scheme.

[9] Using DIA for S_{nl} , the TC96 S_{ds} term was tuned in such a way that the solution of the wave action equation reproduced the observed fetch limited wave growth of the total wave energy [Kahma and Calhoun, 1994] and high-frequency energy level [Hasselmann *et al.*, 1973]. If DIA is simply replaced by SRIAM, dynamic properties of the wave growth

and decay will also be altered because other source functions (S_{in} and S_{ds}) strongly depend on the spectral shape. Therefore, the introduction of SRIAM to WW3 distorts the balance of the source terms and affects the total wave energy. To avoid this, we conducted a preliminary investigation of fetch-limited wave growth and reduced the S_{ds} term by a factor of 0.2 (i.e., $S_{total} = S_{in} + S_{nl}^{SRIAM} + \alpha S_{ds}$, where $\alpha = 0.8$) to reproduce the observational results by *Kahma and Calkoen* [1994], which have been used to tune the default WW3.

2.2. Design of Hindcast Experiments

[10] The computational domain was set to 66°S–66°N latitude and 100°E–290°E longitude, covering the Pacific Ocean except for its polar region. Hindcast was performed for a 1-year integration period in 2004. The wave model was driven by 6-hourly wind stress from the National Centers for Environmental Prediction/National Center for Atmospheric Research (NCEP/NCAR) reanalysis product [*Kalnay et al.*, 1996], in which the global data set has a resolution of 192×94 gaussian grids. Whereas WW3 can incorporate external parameters such as ice concentration, currents, water levels, and air-sea temperature differences, these components were not considered in this study. ETOPO5 [http://www.ngdc.noaa.gov/mgg/global/etopo5.HTML] elevation data were used to define the bottom topography and coastal lines. We ignored shallow-water physics, such as bottom-induced dissipation and modification of the S_{nl} term.

[11] The results of both models (WW3/SRIAM and WW3/DIA) were validated against wave parameters recorded at eight NOAA/NDBC buoys deployed in deep waters, mainly in the northeastern Pacific. Figure 1 gives the locations of the buoys, which fall into three regions: high latitude (46035 and 46066), midlatitude (46005, 46006, 46089), and low latitude (51001, 51004, 51028). Hourly wave fields calculated by the two models were compared to in situ data at the nearest points.

3. Statistical Properties and Wave Spectra of Ocean Waves in the Pacific

[12] In the Pacific, enormous quantities of mechanical wind energy are transferred to surface waves in the midlatitudes from 30° to 60° N and S [e.g., *Wang and Huang*, 2004]. These latitudinal bands correspond to strong surface wind fields associated with storm tracks in the Northern and Southern hemispheres. Ocean waves generated in the midlatitudes propagate far from storms and radiate to lower latitudes as swells. On the other hand, in low latitudes, the tradewinds blowing predominantly from the ENE and ESE constantly generate local windsea. These features characterize the pattern of the surface wind and ocean wave fields in the Pacific.

3.1. Significant Wave Height and Peak Frequency

[13] We first focused on H_s and peak frequency (f_p), which are the basic parameters of wave forecasting. Figure 1 shows typical snapshots of (Figure 1a) H_s and surface wind vectors and (Figure 1b) T_p and peak wave direction in the North Pacific calculated by WW3, with SRIAM representing the S_{nl} term. The spatial distribution of H_s primarily corresponds to synoptic and subsynoptic scale features of surface winds, as shown in Figure 1a. H_s grew up to 9 m, with a peak period of 15 s, inside a storm at midlatitudes (Figures 1a and 1b). Two swell systems generated by individual storms propagated

toward the southeast in the eastern Pacific (Figure 1b). At low latitudes (from 0° to 20° N), the tradewind from the ENE was dominant and H_s reached about 2–3 m, with a peak period of 8–11 s.

[14] Figure 2 shows scatterplot comparisons of (a) H_s and (b) f_p values from the SRIAM and DIA runs. To highlight the differences in model performance in both zonal and meridional directions, we defined four different regions in the North Pacific (WP40N: 35°–45°N, 160°E–180°, WP10N: 5°–15°N, 160°E–180°, EP40N: 35°–45°N, 160°–140°W, EP10N: 5°–15°N, and 160°–140°W). The annual model results for these regions were used for the investigations. The differences in model performance were also quantified in terms of bias (Bias), root mean square error (RMSE), correlation coefficients (CC), and scatter index (SI) [*Cardone et al.*, 1996].

[15] Although there seemed to be some differences in H_s between the SRIAM and DIA runs, the correspondence was quite high (Figure 2a); the CC was always above 99%, and the bias was less than 10 cm in all regions. To implement SRIAM in WW3, the magnitude of the default WW3 S_{ds} term was reduced by a factor of 0.2. This was done to reproduce the observed fetch-limited wave growth, as well as the default WW3 run using DIA to represent the S_{nl} term. In this sense, close correspondence between the models (WW3/SRIAM and WW3/DIA) was apparent. However, we also confirmed for the first time that H_s in a realistic field can also be adequately reproduced by this model setting with SRIAM representing the S_{nl} term and tuning for S_{ds} .

[16] The scatter of f_p was rather large, and the bias and CC differed with longitude and latitude (Figure 2b). The bias of f_p was pronounced in the western Pacific (e.g., WP40N: -0.0057 Hz, EP40N: -0.0035 Hz), whereas in the eastern Pacific the correlation was lower (e.g., WP40N: 88.1%, EP40N: 83.4%), especially in the low-latitude region (EP10N: 82.9%). The scatterplots of f_p also revealed the characteristic frequency dependence of the bias. Peak frequencies calculated by DIA were generally larger (i.e., positive bias) compared to those calculated by SRIAM in the high-frequency region (around 0.09 – 0.15 Hz) at WP10N, EP40N and EP10N. However, scatterplots indicated a persistent positive bias in DIA for the entire frequency domain at WP40N.

[17] We compared the SRIAM and DIA model results to observational data in the eastern Pacific, where the correlation of the peak frequency between the two models was small. The probability density functions (pdfs) of H_s and f_p by SRIAM and DIA are shown in Figures 3 and 4, validated against the in situ data as the ground truth. With the exception of 46089, the computational results by SRIAM and DIA agreed well with each other for H_s (Figure 3). This was consistent with the previous model comparison shown in Figure 2a. Both model results also compared favorably well with the observational results. In middle to high latitudes (46035, 46066, 46005, 46006, and 46089), pdfs of H_s were broadly distributed up to 6–8 m. On the other hand, pdfs were quite narrow and confined to around 2 m in low latitudes (51001, 51004, and 51028). These noticeable tendencies in the pdfs are also present in the model (Figure 2a).

[18] The f_p was distributed with a single peak in the middle to high latitudes (46035, 46066, 46005, 46006, and 46089), while in low latitudes (51001, 51004, and 51028), the pdf of the f_p was characterized by two peak values (Figure 4). Again, the observed pdf features could also be found in the model

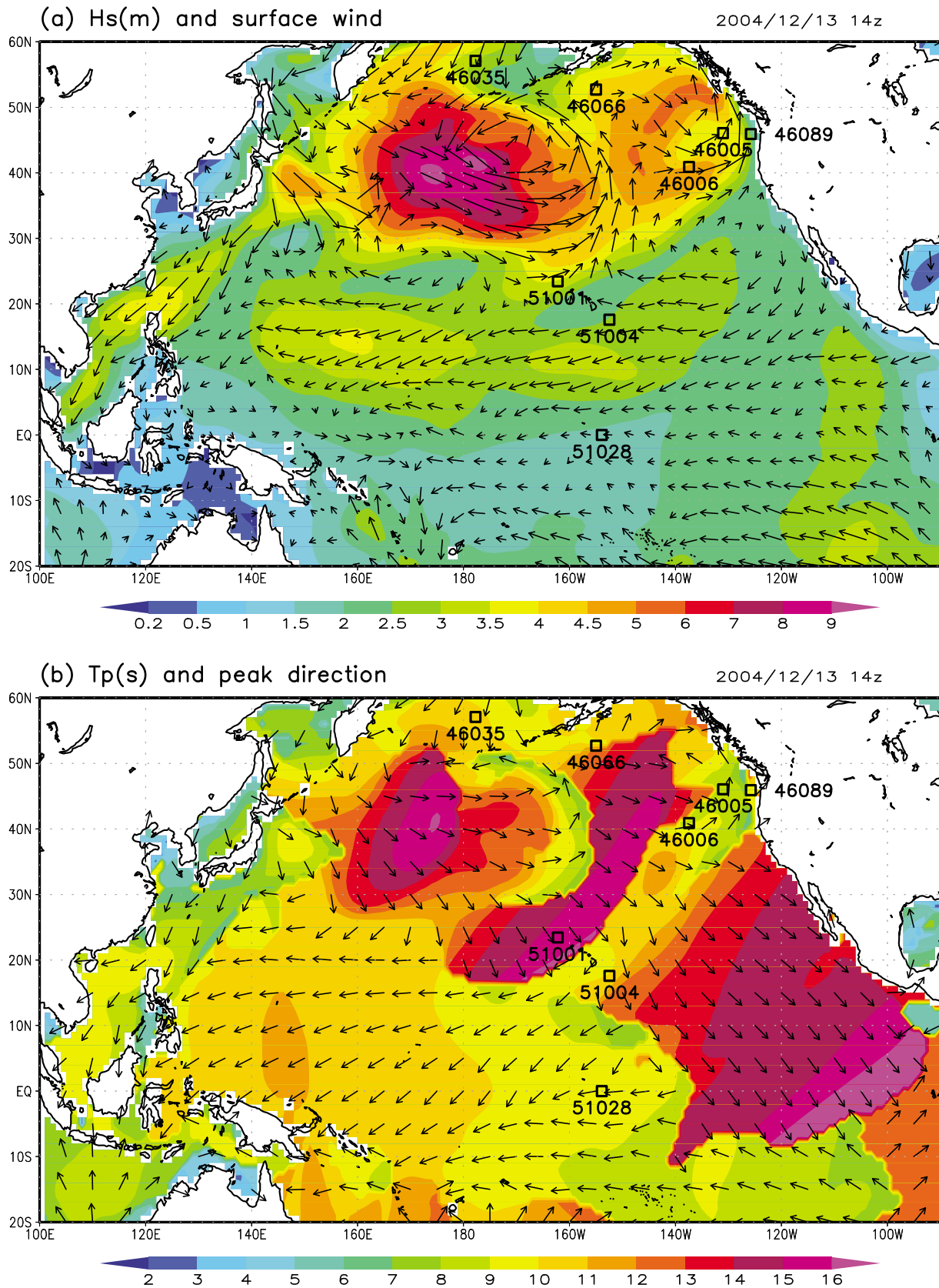


Figure 1. Instantaneous plane view (at 1400 UTC, 13 December 2004) of (a) significant wave height (H_s) and surface wind vectors and (b) peak period (T_p) and peak wave direction in the North Pacific calculated using SRIAM for the S_{nl} term. Squares show the locations of the NDBC buoys used in the analysis, which included data for a 1-year integration period.

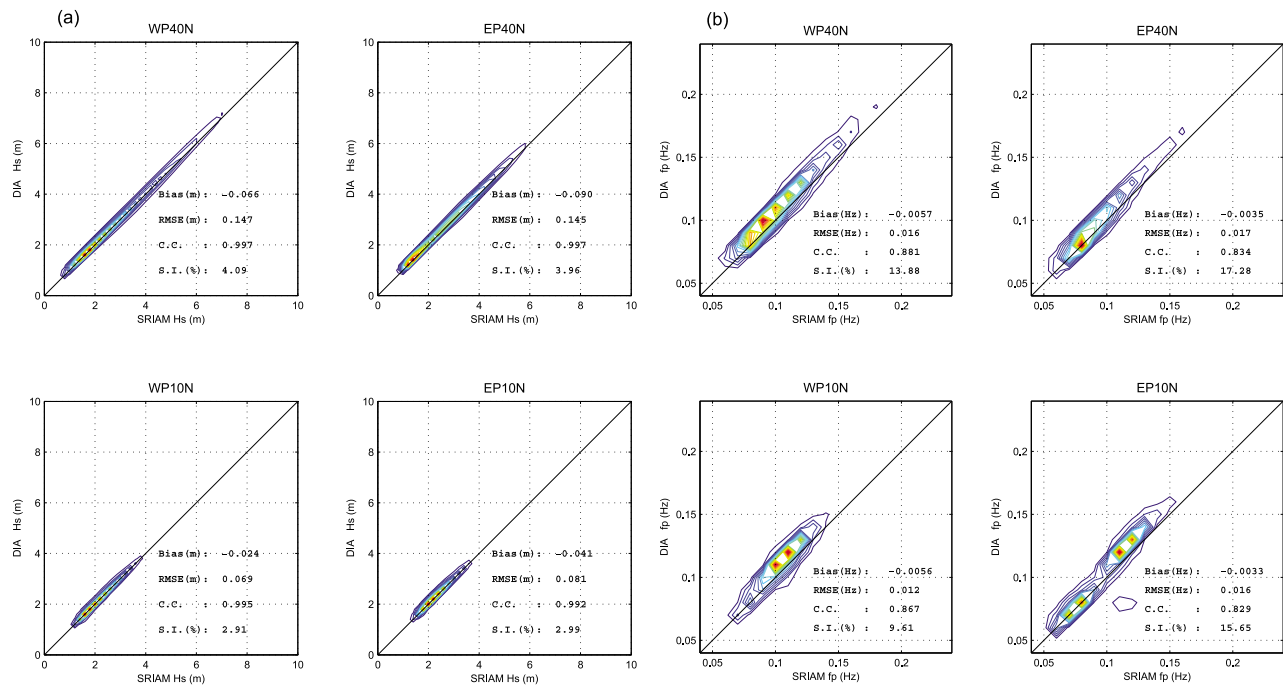


Figure 2. Scatterplot comparison of (a) H_s and (b) f_p for the SRIAM and DIA values for four different regions in the North Pacific (WP40N: 35°N–45°N, 160°E–180°, WP10N: 5°N–15°N, 160°E–180°, EP40N: 35°N–45°N, 160°W–140°W, EP10N: 5°N–15°N, 160°W–140°W). Annual model results over these regions are used for the investigations. The contour interval is 0.1 in units of maximum values.

(Figure 2b). In midlatitudes in the eastern Pacific (EP40N), the model f_p was continuously distributed from about 0.06 Hz to 0.15 Hz, as confirmed by observations at 46066, 46005, and 46006. However, the pdf of the model f_p has a local minimum around 0.1 Hz in EP10N, which was the same as that observed at 51001, 51004, and 51028 (Figure 4). In addition, the f_p at EP10N (Figure 2b) calculated using DIA indicated a positive bias around f_p values greater than 0.1 Hz. For f_p values less than 0.1 Hz, the bias became small. The reproducibility of this bimodality of the peak frequency manifested as a pronounced difference in the performance of the two models (Figure 4). SRIAM successfully captured this bimodality of the pdf while DIA indicated bimodality but gave values that were not consistent with observations for the high-frequency peak (greater than 0.1 Hz). The differences between the pdfs were statistically significant at the 5% significance level using a two-sample Kolmogorov-Smirnov test.

[19] We further quantified the performance of the two models against observations using various statistical scores (Table 1). Both models performed well for H_s . The differences in RMSE and CC were within a few centimeters and 0.01, respectively, at any buoy location. However, the prediction skills of H_s seemed to depend on location. They were not significantly improved using SRIAM. SRIAM had consistently better f_p values than DIA, but the difference in the verification scores (RMSR, CC and SI) were rather small. In the low-latitude region (51001, 51004, and 51028), f_p also improved (χ^2 values are shown in Table 1). It is also interesting to note that the default parameterization of WW3/DIA had a tendency to overestimate (underestimate) the f_p (T_p) for moderate to strong wind fields, as was seen in *Chao et al.*

[2005] and *Padilla-Hernández et al.* [2007]. Our results also suggest the same features; f_p calculated by DIA indicated positive bias with the exception of 46089, whereas f_p calculated by SRIAM indicated random variance with small bias.

[20] In summary, these results can be explained physically as follows. In the midlatitude Pacific, the pdf of H_s is broadly distributed because of the prominent westerlies and the strong variation in surface wind associated with storm tracks. The f_p is continuously distributed in this region (Figures 2b and 4), and its spread may be accounted for by the strong variation in local winds. In other words, in midlatitudes, the predominant local windsea distribution is not significantly affected by swells. Swells coming from the windsea source regions in the midlatitudes propagate toward low latitudes, particularly the eastern tropical and subtropical region of the Pacific (Figure 1b). In addition, the surface winds are steadier and more moderate than those at high latitudes. The pdfs of H_s at low latitudes are quite narrow and confined, as shown in Figures 2a and 3. This is because the swells and windsea energies are of the same order of magnitude. The pdf of f_p is clearly separated into two peak values; the lower-frequency peak corresponds to swells from high latitudes, while the higher-frequency peak corresponds to local windsea induced by the trade wind. Evaluation of the spectral peak due to trade winds seems to improve when SRIAM is used. These features of wave fields in the North Pacific were also confirmed in the spectral evolution and associated wave parameters, as described below.

3.2. Wave Spectral Properties

[21] Figure 5 presents a typical winter time-series comparison of physical parameters in the midlatitude Pacific

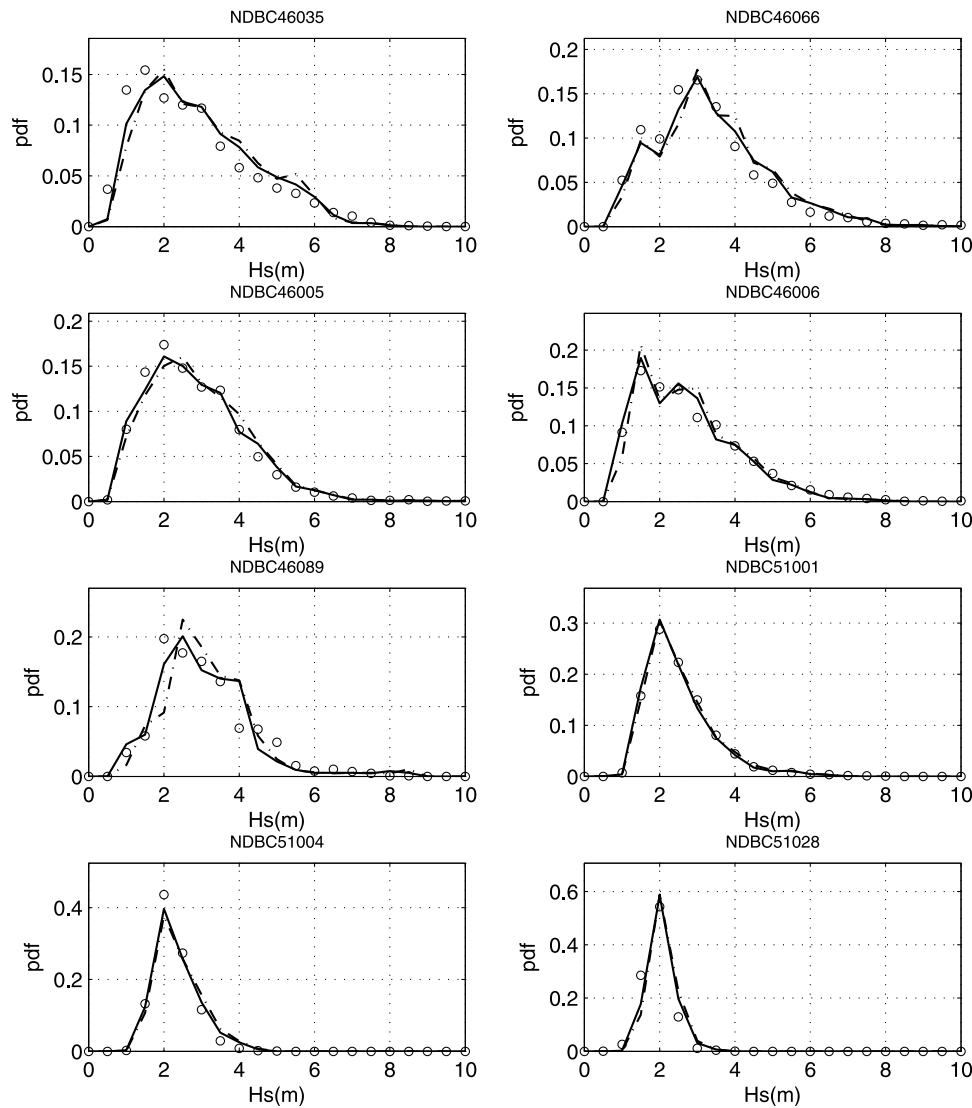


Figure 3. The probability density functions of H_s calculated by SRIAM (solid line) and DIA (dashed-dotted line) with in situ data (circle) for each location.

(NDBC 46006), showing (Figure 5a) wind speed and H_s , (Figure 5b) in situ wave spectra normalized by peak spectral energy ($F_p^{\text{obs}} / F_p^{\text{obs}}$), (Figure 5c) normalized wave spectra calculated by SRIAM ($F_p^{\text{SRIAM}} / F_p^{\text{SRIAM}}$), and (Figure 5d) the difference in normalized wave spectra between SRIAM and DIA ($(F_p^{\text{SRIAM}} - F_p^{\text{DIA}}) / F_p^{\text{SRIAM}}$), where F is the one-dimensional wave spectrum in the frequency domain and F_p is the peak spectral energy. Storms induced significant fluctuations in wind speed during the 12 days from 3 to 15 December. Thereafter wind speed gradually decreased from 16 to 25 December and then increased again rapidly due to two storms between 25 and 31 December. The H_s calculated by the wave models showed close agreement with the observational data, with the exception of 4 and 12–13 December, which may have been due to errors in surface wind forcing.

[22] The shapes of wave spectra changed rapidly in the midlatitudes, and this was associated with temporal changes in local wind fields. The time evolution of wave spectra (shown in Figure 5c) was characterized by strong downshifting (indicated by black bars) and weak upshifting (indicated by red bars) of

the spectral peak. The former corresponded to wave development due to the strong local wind field, in which S_{nl} induced downshifting of the spectral peak. The latter corresponded to swell propagation, in which longer swells arrived first, followed by shorter swells due to wave dispersion. In addition, storms induced rapid spectral transformation within a few hours (indicated by blue bars). Swells also coexisted with local windsea from 4 to 19 December, indicating spectral evolution in a mixed sea state.

[23] The differences in spectral energy between SRIAM and DIA (Figure 5d) were persistent around the spectral peaks during the periods indicated by the blue and black bars. Negative and positive differences in the spectral energy across the spectral peaks suggest that the peak frequencies of DIA are shifted to high frequencies. This is also observed in Figure 2b, where the default WW3 tends to indicate a positive bias for f_p . This feature was also suggested in previous studies [e.g., Chao *et al.*, 2005; Padilla-Hernández *et al.*, 2007; Xu *et al.*, 2007]. In addition, DIA fails to reproduce the spectral shape around the spectral peak, as discussed in the next section.

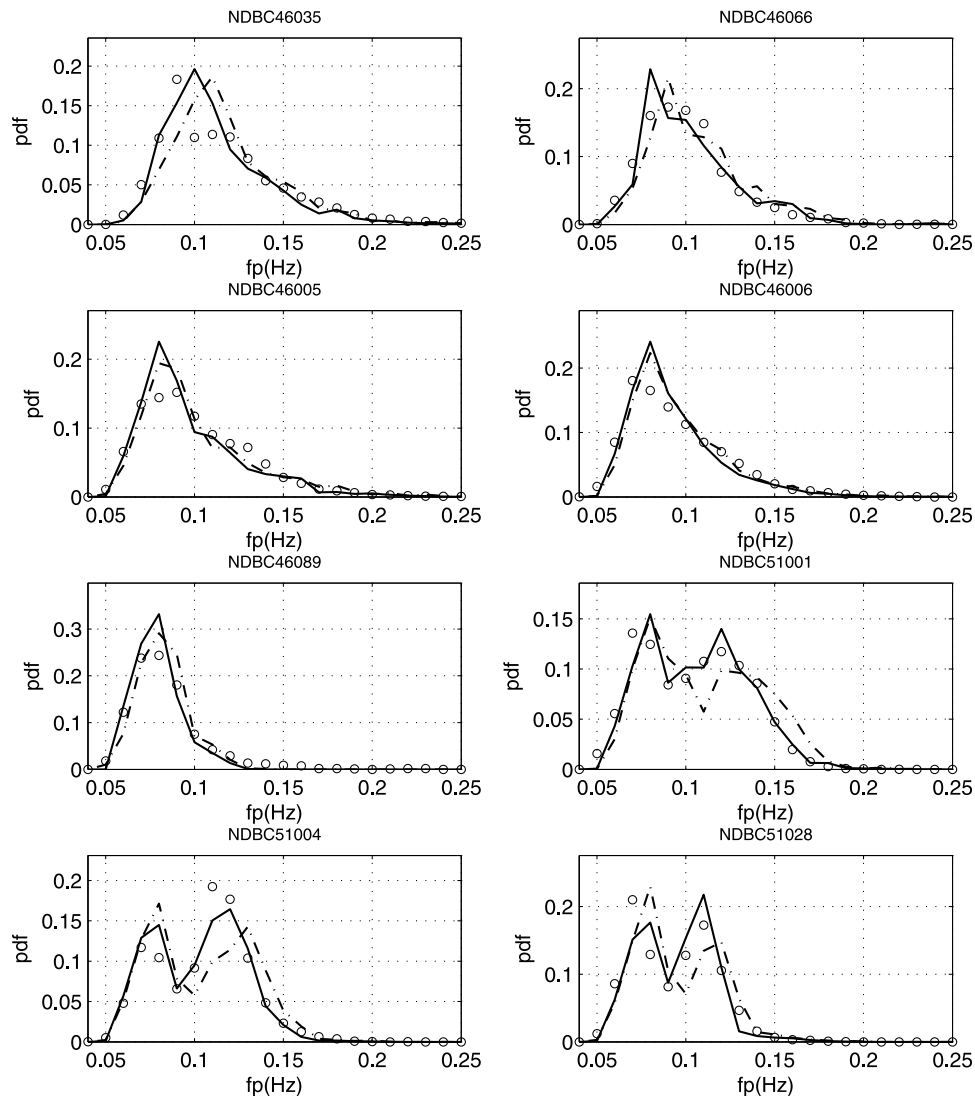


Figure 4. Same as Figure 3, but for peak frequency.

[24] The two-dimensional (2-D) wave spectra clearly differed between SRIAM and DIA. Figure 6 presents wave spectral energy densities for “pure” windsea in the frequency and directional domain at 0:00 on 26 December. Around the spectral peak, the 2-D wave spectrum calculated by DIA (Figure 6b) is much broader, especially in directional space, than that by SRIAM (Figure 6a). In addition, a bimodal distribution appears on the low-frequency side of the peak frequency. That is, DIA redistributes wave energy at much larger oblique angles than expected with exact nonlinear transfer, which is a recognized shortcoming of DIA [Komatsu and Masuda, 1996; Van Vledder, 2006b; Tamura et al., 2008].

[25] Figure 7 presents typical examples of the time history of wave parameters in the low-latitude Pacific (NDBC 51004). At low latitudes, the surface wind speed fluctuated only gradually around 8 m/s, and the estimated H_s calculated by SRIAM and DIA compared well with observations (Figure 7a). The H_s time series indicated a gradual transition compared to the case at higher latitudes, owing to the different atmospheric conditions. The time evolution of the observed wave spectra (Figures 7b

and 7c) was characterized by persistent spectral peaks around 0.12 Hz (indicated by yellow bars) and slowly upshifting spectral peaks from 0.05 to 0.1 Hz (indicated by red bars). The former corresponded to the windsea induced by the steady tradewind blowing from the ENE, whereas the latter corresponded to swell propagation from higher latitudes. This bimodal behavior of f_p values corresponding to the windsea and swell resulted in the bimodality of the pdf in Figure 2b (EP10N) and Figure 4.

[26] The clearest difference between the models was the peak frequency associated with the tradewind (i.e., higher peak frequency); DIA clearly overestimated the observed peak while SRIAM reproduced this peak reasonably well (Figures 4 and 7d). Again, this difference was easily confirmed in the 2-D wave spectrum, where four local maxima of spectral energy were seen (Figure 8). The local maxima of the windsea at frequencies greater than 0.1 Hz were shifted to higher frequencies with DIA as compared to SRIAM, while the swell peaks at frequencies less than 0.1 Hz were consistent for both models. These features were also apparent in the differences

Table 1. Summary of the Bulk Model Statistics for (A) Significant Wave Height and (B) Peak Frequency

| (a) | | | | | | | | | | | |
|----------|------|-------------|------------|-------------|-------------|-------------|-------------|-------------|-------------|-----------------|-------------|
| Location | Data | Bias (cm) | | RMSE (m) | | CC | | SI (%) | | χ^2 values | |
| | | SRIAM | DIA | SRIAM | DIA | SRIAM | DIA | SRIAM | DIA | SRIAM | DIA |
| 46035 | 8753 | 19.5 | 26.8 | 0.71 | 0.74 | 0.90 | 0.90 | 24.8 | 25.0 | 548.4 | 869.3 |
| 46066 | 4151 | 15.0 | 21.7 | 0.73 | 0.72 | 0.89 | 0.90 | 22.1 | 21.2 | 167.8 | 278.9 |
| 46005 | 8600 | 6.2 | 14.2 | 0.62 | 0.63 | 0.89 | 0.89 | 22.0 | 21.8 | 164.1 | 235.2 |
| 46006 | 8761 | -12.4 | -3.3 | 0.54 | 0.54 | 0.93 | 0.92 | 18.8 | 19.0 | 221.6 | 387.4 |
| 46089 | 1169 | -3.6 | 10.0 | 0.62 | 0.62 | 0.87 | 0.87 | 20.2 | 20.1 | 223.1 | 340.7 |
| 51001 | 7549 | -5.5 | 1.0 | 0.40 | 0.41 | 0.91 | 0.90 | 15.5 | 16.0 | 86.2 | 73.4 |
| 51004 | 8744 | 9.4 | 15.2 | 0.38 | 0.40 | 0.79 | 0.79 | 16.3 | 16.6 | 639.5 | 1240.9 |
| 51028 | 8723 | 13.4 | 17.8 | 0.33 | 0.35 | 0.61 | 0.62 | 15.9 | 15.8 | 1189.7 | 2122.3 |

| (b) | | | | | | | | | | | |
|----------|------|----------------|----------------|--------------|--------------|-------------|-------------|-------------|------|-----------------|--------------|
| Location | Data | Bias (Hz) | | RMSE (Hz) | | CC | | SI (%) | | χ^2 values | |
| | | SRIAM | DIA | SRIAM | DIA | SRIAM | DIA | SRIAM | DIA | SRIAM | DIA |
| 46035 | 8753 | -0.0025 | 0.0030 | 0.032 | 0.034 | 0.52 | 0.49 | 27.4 | 29.1 | 1068.2 | 1241.9 |
| 46066 | 4151 | 0.0018 | 0.0071 | 0.025 | 0.029 | 0.55 | 0.51 | 25.0 | 27.7 | 348.3 | 559.2 |
| 46005 | 8600 | -0.0029 | 0.0009 | 0.030 | 0.032 | 0.53 | 0.51 | 29.5 | 31.3 | 772.6 | 610.3 |
| 46006 | 8761 | -0.0017 | 0.0017 | 0.028 | 0.030 | 0.47 | 0.44 | 29.5 | 31.2 | 650.3 | 574.3 |
| 46089 | 1169 | -0.0050 | -0.0020 | 0.022 | 0.021 | 0.42 | 0.42 | 25.0 | 25.2 | 141.6 | 121.9 |
| 51001 | 7549 | 0.0026 | 0.0069 | 0.025 | 0.028 | 0.63 | 0.61 | 23.6 | 25.7 | 344.4 | 1575.9 |
| 51004 | 8744 | -0.0026 | 0.0001 | 0.024 | 0.027 | 0.54 | 0.50 | 23.1 | 25.7 | 367.8 | 1729.1 |
| 51028 | 8723 | 0.0018 | 0.0029 | 0.024 | 0.025 | 0.43 | 0.44 | 25.4 | 26.8 | 808.1 | 1647.4 |

in pdfs (Figure 4). The discrepancy in the high-frequency peaks is mainly because the default WW3 has a persistent bias and overestimates of peak frequencies under moderate wind conditions. Other possible reasons for this include a well-known problem of DIA: It fails to adequately calculate the energy transfer of bimodal wave spectra [e.g., *Young and Van Vledder*, 1993; *Komatsu and Masuda*, 1996; *Van Vledder et al.*, 2000]. In addition, the spectral bandwidth around the peak was narrow for the SRIAM runs, correcting the well-known DIA shortcoming of tending to broaden the wave spectrum around the spectral peak in the frequency and directional domains.

3.3. Spectral Shape Parameters

[27] The frequency peakedness Q_p [*Goda*, 2000] is defined as follows:

$$Q_p = 2m_0^{-2} \int_0^\infty f \left[\int_0^{2\pi} F(f, \theta) d\theta \right]^2 df, \quad (1)$$

where $F(f, \theta)$ is the wave spectrum defined in the frequency-directional domain and m_0 is the total spectral energy. Q_p provides an adequate indication of the structure and evolution of wave spectra in the frequency domain (note that *Van Vledder and Battjes* [1992] and *Goda* [2000] questioned the applicability of Q_p regarding spectral smoothing and resolution). Recent studies have indicated that seas with a high probability of freak wave occurrence can be parameterized by wave steepness and the spectral bandwidths in frequency and direction. Therefore, Q_p is a relevant parameter for identifying seas with a high chance of freak waves [*Janssen and Bidlot*, 2003; *Waseda et al.*, 2009a; *Tamura et al.*, 2009]. We compared the model results on the basis of SRIAM and DIA with observational data where in situ Q_p values were defined from the frequency spectra of the specific NDBC buoys.

[28] Figures 9a and 9b show time series of Q_p for the same duration and location as in Figures 5 and 7. In general, the Q_p estimated by SRIAM was larger than that estimated by DIA because SRIAM improves the shortcomings of DIA. DIA tends to broaden the spectra in the frequency domain compared to rigorous algorithms for S_{nl} [e.g., *Hasselmann et al.*, 1985]. The most pronounced difference between the model results and in situ data appeared during the passage of swells. The Q_p s calculated by the two models showed abrupt changes around 2 and 22 December (Figure 9a). Thereafter, they maintained higher values for a few days more than in other periods. This is attributable to the propagation of swells over long distances; quite a narrow spectrum appears in the low-frequency region (< 0.1 Hz) in Figures 5b and 5c. While the time series of in situ Q_p s (open circles) did not show these changes, that of the modeled frequency spectrum actually captured the swell propagation at that time (see Figures 5b and 5c). Similar in situ Q_p fluctuations were observed at other times at this location.

[29] The main reason for this discrepancy might be the coarse frequency resolution of the observed wave spectra (Figure 9a, NDBC 46006 in December). That is, the Q_p parameter is strongly dependent on the resolution of the wave spectrum, which is a recognized shortcoming, as discussed by *Goda* [2000]. In this case, the in situ frequency spectrum was given by a frequency bin size of 0.01 Hz in the range 0.03–0.4 Hz. The spectral resolution was insufficient to estimate Q_p for the quite narrow spectrum, especially in the low-frequency region.

[30] On the other hand, the in situ Q_p in low latitudes calculated using a higher-resolution spectrum (Figure 9b, NDBC 51004 in April) showed reasonable agreement with the computational results, especially those of SRIAM (Figure 9b), for swells propagating at this location (on 8 and 27 April). The wave spectra obtained by NDBC buoy 51004

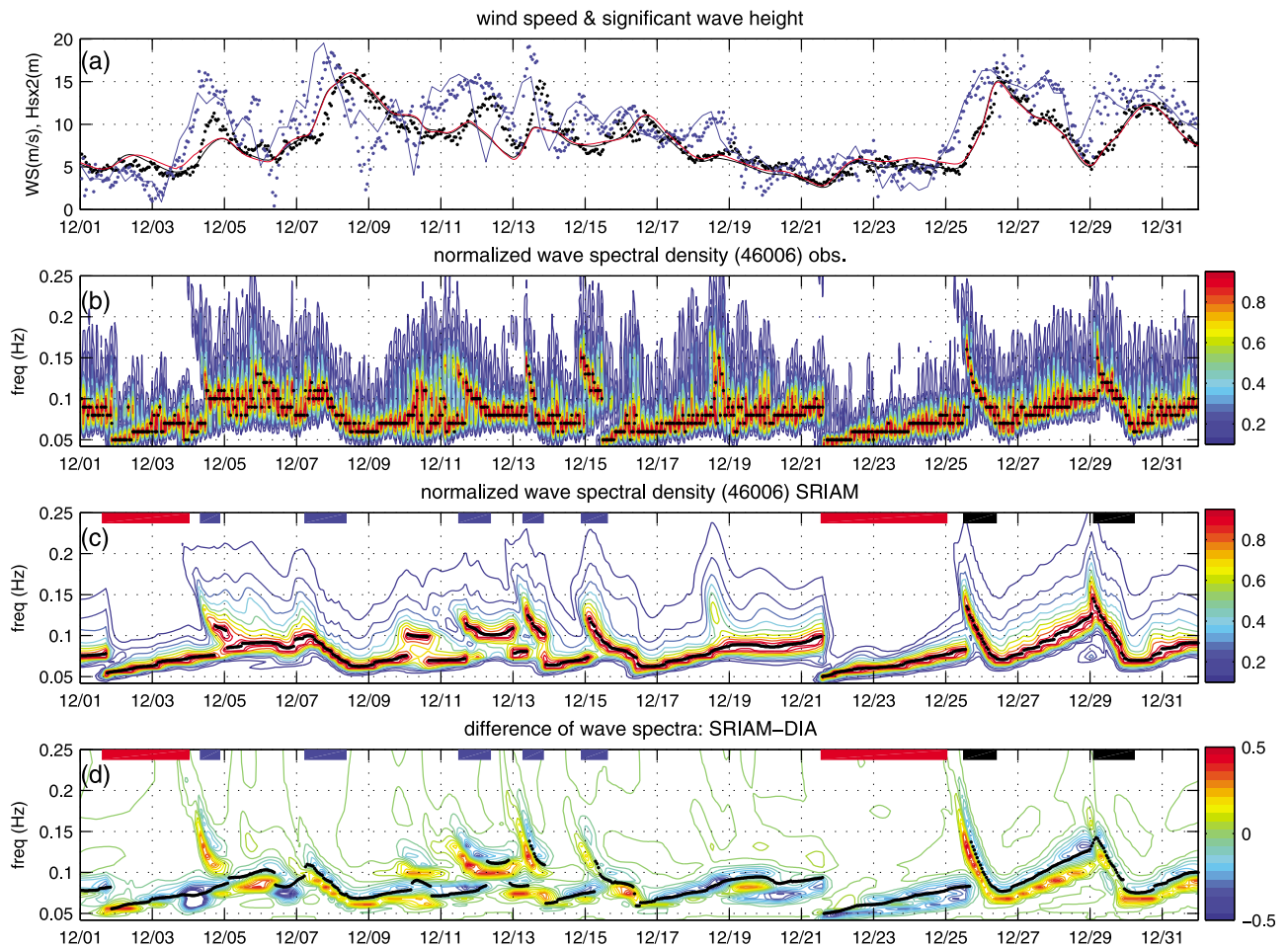


Figure 5. Time series of physical parameters at the NDBC 46006 buoy in the midlatitude Pacific. (a) Wind speed (blue line: NCEP/NCAR reanalysis, blue dots: NDBC obs.) and significant wave height H_s (black line: SRIAM, red line: DIA, black dot: NDBC obs.), (b) normalized in situ wave spectra (NDBC obs.), (c) normalized wave spectra and f_p calculated by SRIAM, and (d) the difference in spectral energy between SRIAM and DIA with f_p calculated by DIA. All data are plotted hourly. Frequency spectra (b and c) and the difference of spectra (d) were normalized by the peak spectral energy using SRIAM at each time point. The contour interval is 0.1 in units of maximum values for (b) and (c) and is ± 0.05 in units of maximum absolute value for (d).

(Figure 7b) were narrow in the frequency domain for 8 and 27 April. On these days, in situ Q_p values showed pronounced peaks (Figure 9b). In this case, the Q_p calculations by the two models also captured the near-maximum value for the 2 days, although DIA underestimated these peak values. The Q_p obtained by SRIAM was clearly underestimated for the period from 11 to 21 April. This was because there were many more swells with a frequency lower than 0.1 Hz during this period in the SRIAM simulation (Figure 7c) than in the in situ spectra (Figure 7b). In reality, these artificial swells ought to be attenuated by the sheltering effect of small islands [Tolman, 2003].

4. Wave Spectral Shape and Source Balance in Growing Windsea

[31] The wave spectra in a growing windsea are mainly characterized by overshooting around the spectral peak and

power law behavior in the equilibrium range. The self-similar spectra of ocean surface waves are considered to possess these properties.

[32] *Barnett and Wilkerson* [1967] observed characteristic spectral growth in the fetch-limited evolution of wind waves and named it the “overshoot effect”. When the growth of a particular spectral component is traced along the fetch, the energy of this component oscillates between overshoot and undershoot before reaching final equilibrium. *Mitsuyasu* [1969] provided an explanation for the “overshoot effect” in fetch-limited conditions in relation to the excess energy concentration near the dominant peak of the wave spectrum. *Hasselmann et al.* [1973] also reported that the mean spectral shape measured in the Joint North Sea Wave Project (JONSWAP) agreed well with findings of previous studies [e.g., *Barnett and Wilkerson*, 1967; *Mitsuyasu*, 1969] and suggested that nonlinear energy transfer controlled the development of the pronounced peak. The physical mechanism of

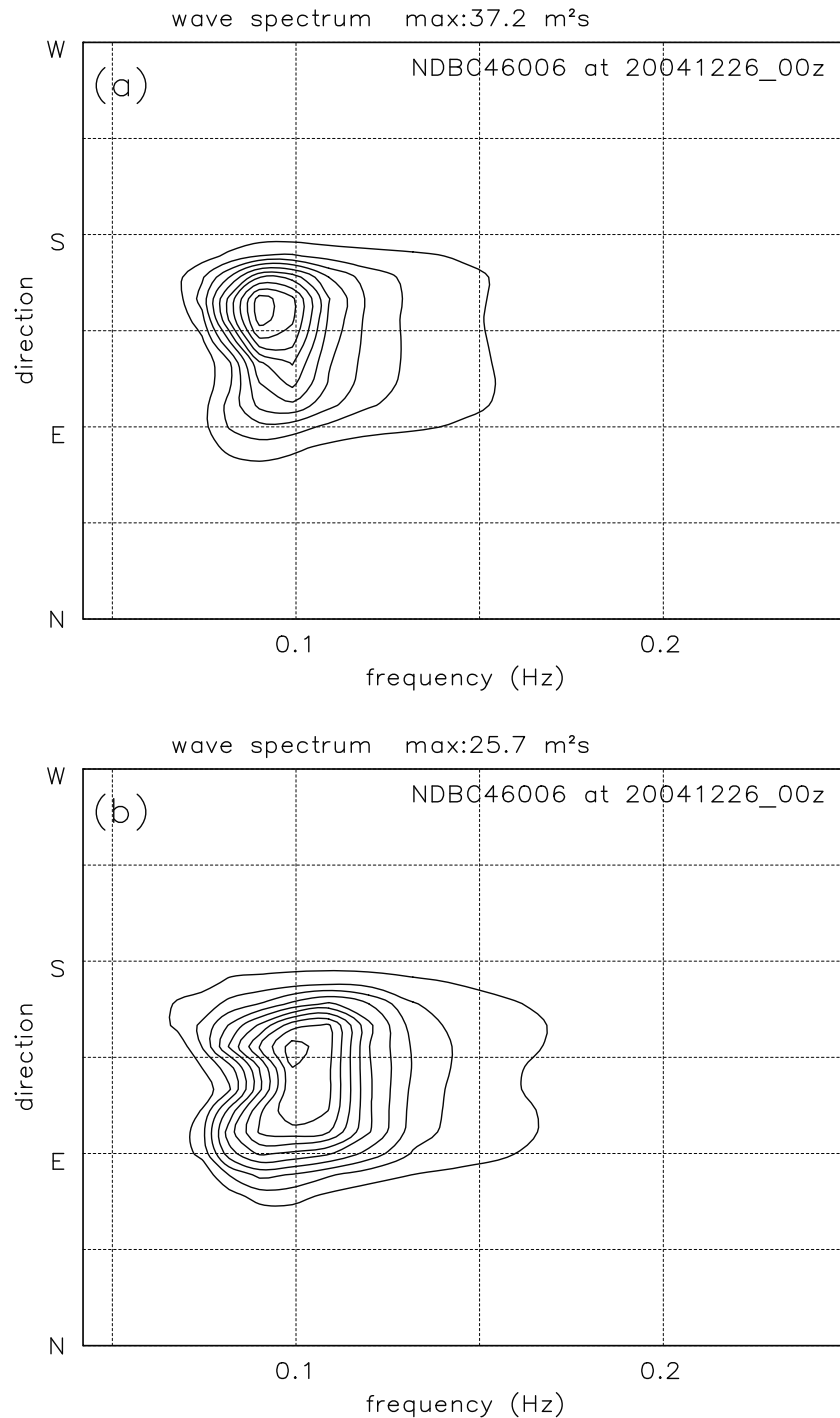


Figure 6. Frequency-direction wave spectra at 0:00, 26 December (NDBC 46006) obtained by (a) SRIAM and (b) DIA. The contour interval of the wave spectra is 0.1 in units of maximum wave spectrum.

the overshoot phenomenon was explained by *Holthuijsen* [2007] in terms of the relative role of the source functions.

[33] In addition, both observational and laboratory studies have indicated the existence of an equilibrium range in which the wave spectrum follows the f^{-4} power law [*Zakharov and Filonenko*, 1966; *Toba*, 1973]. The physical mechanisms responsible for the formation of the equilibrium range have remained obscure, although possible mechanisms have been discussed by many researchers [e.g., *Kitaigorodskii*, 1983;

Phillips, 1985; *Pushkarev et al.*, 2003; *Badulin et al.*, 2005]. *Kitaigorodskii* [1983] suggested the primary importance of S_{nl} , which transports wave energy from low to high frequencies in the equilibrium region. In contrast, *Phillips* [1985] suggested that the three source terms are all of the same order of magnitude and balance one another. Many arguments have been presented regarding the relative roles of the source terms. Nevertheless, these studies have suggested

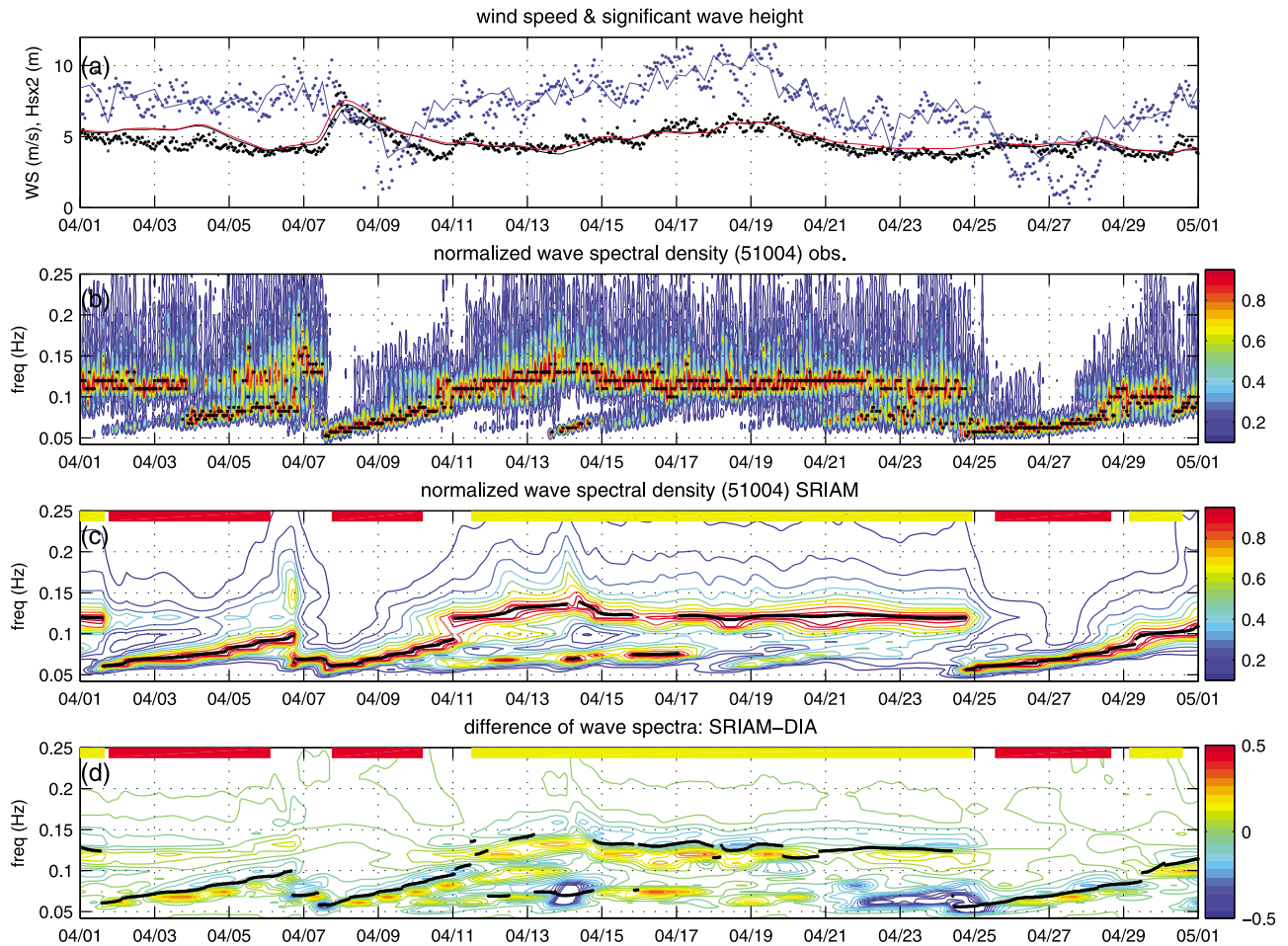


Figure 7. Same as Figure 5, but at NDBC 51004 in the low-latitude Pacific.

that the S_{nl} term may be of central importance to the wave generation process in the equilibrium range.

[34] Third-generation wave models can represent the pronounced peak due to nonlinear transfer [e.g., *Komen et al.*, 1994] and have successfully reproduced the f^{-4} power law in the equilibrium range using a proper S_{nl} model [e.g., *Resio and Perrie*, 1991; *Komatsu and Masuda*, 1996]. Therefore, third-generation wave models have great potential for the evaluation of wave spectra. As presented in the following section, we analyzed point data from buoy 46006 in the midlatitude region to investigate the properties of a growing windsea. Because the analysis integrated data for a yearlong period, we believe that it captures the principal features of a growing sea and does not lose generality. We investigated in detail the mean spectral shape obtained by the hindcast experiments and compared that to observed NDBC spectra.

4.1. Mean Wave Spectra

[35] Figure 10 presents the mean and standard deviation of the wave spectra at buoy 46006 (Figure 10a), calculated by SRIAM (Figure 10b) and DIA (Figure 10c). To investigate the higher frequency part of the spectra, the wave spectra were normalized as follows:

$$\Phi(f/f_p) = F(f)f^4/gu_{10}, \quad (2)$$

where F is the frequency spectrum, g is gravitational acceleration, and u_{10} is wind speed at 10 m height. If the wave spectrum obeys f^{-4} shape, the normalized spectrum (or saturation spectrum) Φ attains a steady value in the high-frequency region. The wave spectra were selectively analyzed for a young windsea with a unimodal peak; the inverse wave age (defined as u_{10}/c_p , with c_p being the phase speed of the spectral peak) was greater than 1, and the spectral shape had one local maximum value. Normalized wave spectra (2) were averaged for discrete bins of $\Delta f/f_p = 0.1$. The wind speed observed at 5 m at the NDBC buoy was adjusted to 10 m by applying the 1/7 wind profile power law. The mean wave spectra shown in Figure 10 reflect well-known behaviors of wave spectra in the windsea; these were classified on the basis of two types of features, depending on frequency range: 1) overshoot, undershoot, and the associated spectral bandwidth around the peak frequency region ($f/f_p < 1.5$); and 2) spectral shapes, such as a small hump at about twice the f_p and a high-frequency tail in the equilibrium range ($f/f_p > 2$).

[36] The wave spectra measured by the NDBC buoy exhibited overshoot ($f/f_p \sim 1.0$) and undershoot ($f/f_p \sim 1.3$) around the spectral peak. SRIAM (Figure 10b) but not DIA (Figure 10c) reproduced these phenomena well. DIA clearly overestimated overshoot as well as the energy levels for frequencies lower than f_p . In addition, the frequency at the undershoot point was shifted to the higher-frequency side

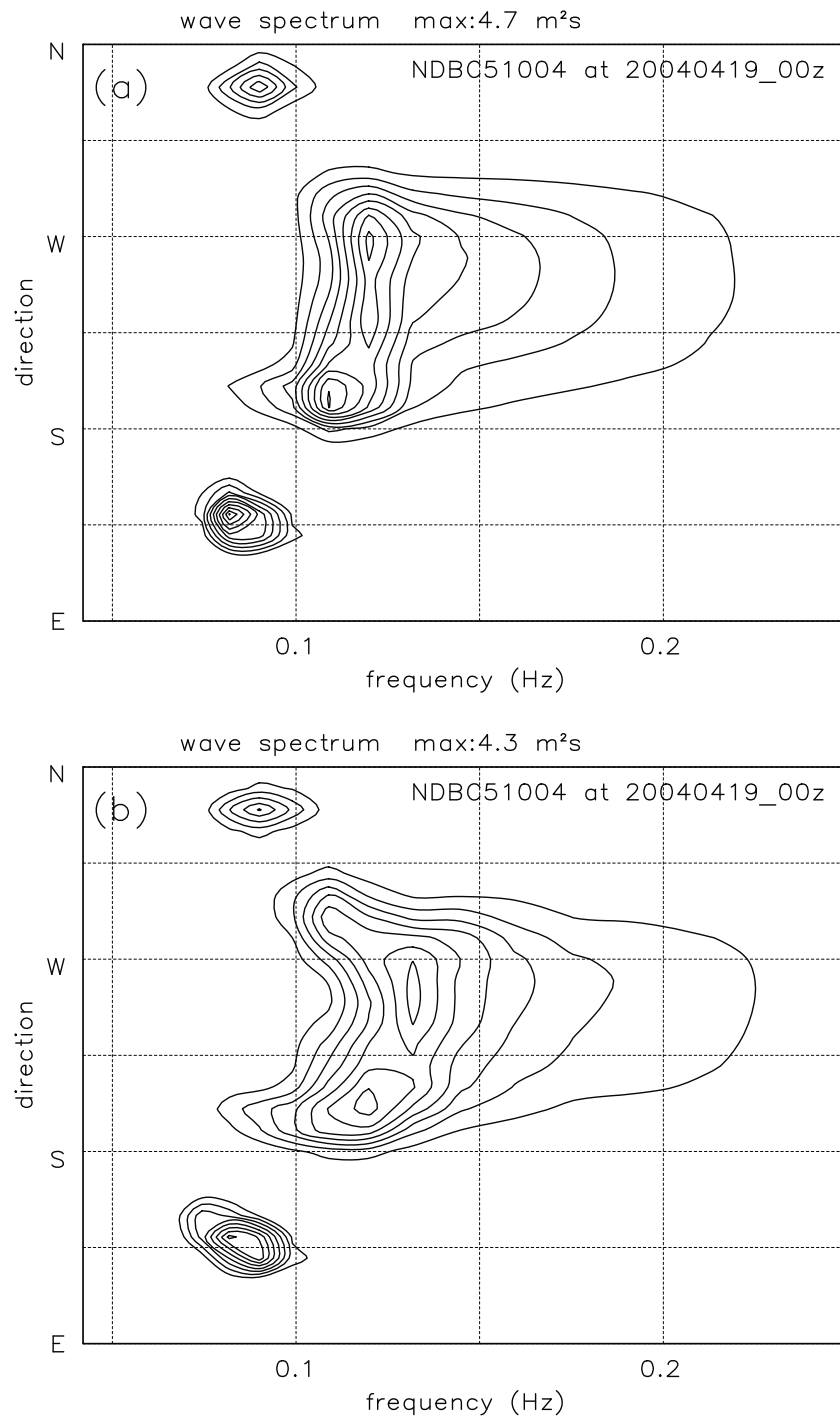


Figure 8. Frequency-direction wave spectra at 0:00, 19 April (NDBC 51004) obtained by (a) SRIAM and (b) DIA. The contour interval of the wave spectra is 0.1 in units of maximum wave spectrum.

around $f/f_p \sim 1.4$. In contrast, SRIAM reproduced the energy level around the spectral peak as well as the frequency at the undershoot spectrum ($f/f_p \sim 1.3$) more realistically. These differences also affected the spectral bandwidth results of each model. That of DIA was much broader than that of the in situ spectrum, whereas SRIAM quantitatively reproduced the spectral bandwidth around the peak frequency.

[37] In the equilibrium range (e.g., f/f_p : from 2 to 3), the in situ wave spectrum indicated power law behavior

(Figure 10a), in which the saturation spectrum Φ was nearly constant and the spectral tail seemed to obey the f^{-4} power law (or the power law with a slightly smaller exponent than -4). In addition, there appeared to be a small local peak at $2f_p$. This small hump at about twice the value of f_p appeared for inverse wave ages greater than 1 (Long and Resio [2007], their Figure 10), suggesting that wave development is important for the generation of this small hump. In the higher-frequency region ($f/f_p > 3$), the spectral tail gradually diverged

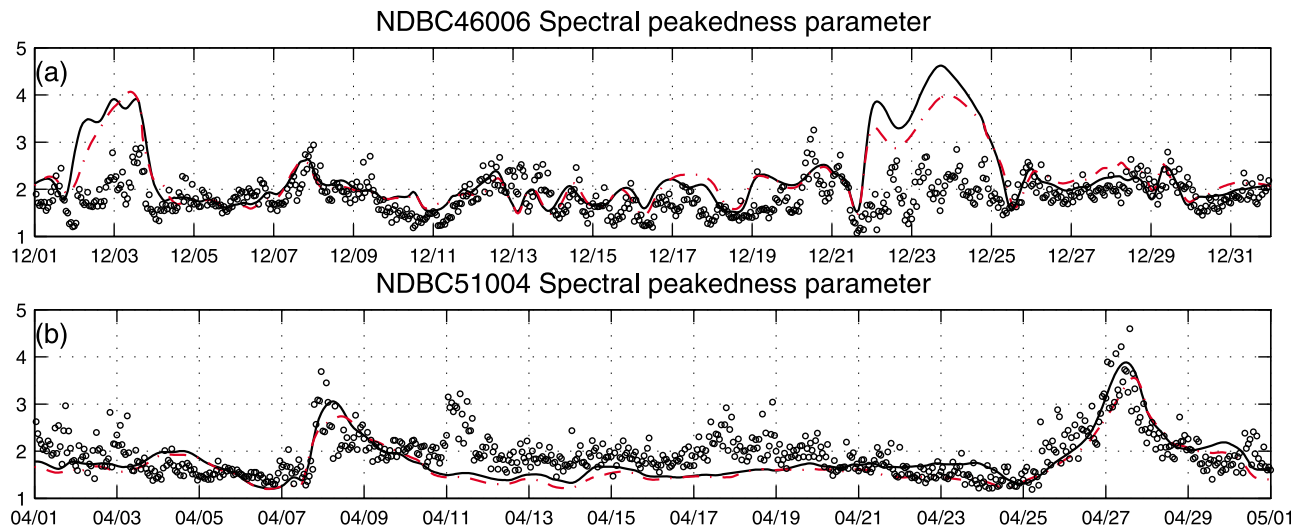


Figure 9. Time series of frequency peakedness Q_p at (a) NDBC 46006 and (b) NDBC 51004, which correspond to Figures 4 and 5, respectively, at the same duration and location; circle: in situ data, solid black line: SRIAM, dashed-dotted line: DIA. In situ Q_p was calculated from historical NDBC data with (a) lower-frequency resolution of 0.01 Hz bin size and with (b) higher-frequency resolution of 0.005–0.02-Hz bin size, respectively.

from the f^{-4} power law and sloped downward. Similar patterns of the deviation from f^{-4} spectral shapes were confirmed by *Resio et al.* [2004; hereafter RLV04] and *Long and Resio* [2007]. It is possible that this is either the manifestation of the dissipation-controlled wave spectral slope [*Hansen et al.*, 1990] or measurement error due to the size of the buoy (3 m disc buoy). Therefore, we do not discuss the spectral shape in the frequency range higher than $3.5 f_p$.

[38] The effect of the accuracy of S_{nl} parameterization on the spectral tail slope was not as direct as that of the spectral shape around the peak frequency. The spectral tail calculated by DIA clearly followed an alternative power law such as f^{-5} in the equilibrium range ($f/f_p > 2$) instead of f^{-4} . On the other hand, the spectral tail by SRIAM seemed to approach the observational result and tended to follow the $f^{-4.5}$ power law in contrast to the spectral tail of DIA. TC96 developed the wave dissipation term based on the new concept that wave dissipation should be separated into at least two scales explicitly for the spectral peak (low-frequency dissipation) and for the equilibrium range (high-frequency dissipation). Furthermore, TC96 developed the high-frequency dissipation so that the spectral tail obeys the f^{-3} power law in the equilibrium range. Therefore, the spectral tail indicated in Figure 10c is an expected result of the original WW3; however, the model did not reproduce the observational results. On the other hand, the spectral tail calculated by SRIAM seemed to have an improved spectral shape as compared to observations. However, as discussed later, the S_{ds} term is an important factor in determining the spectral form in the higher-frequency region.

[39] It is also worth mentioning that both model results show a hump at about twice the peak frequency that also appears in the NDBC buoy data. However, this should not be interpreted as physically sound model behavior. TC96 indicated that an artificial local peak of the wave spectrum appears in the transition zone between high- and low-

frequency dissipation models (Figure 8b in TC96). Our model results also indicate the same physically incorrect behavior.

4.2. Source Terms and Their Balance

[40] Following RLV04, we investigated the relationship between wave spectral shape and source term balance. To maintain the equilibrium range, the sum of the three source terms should be zero within the equilibrium range, as follows:

$$S_{in} + S_{ds} + S_{nl} = S_f - \partial\Gamma_E/\partial f = 0, \quad (3)$$

where S_f is the net external force due to wind input and dissipation (i.e., $S_{in} + S_{ds}$), and Γ_E is the net flux of energy due to the nonlinear interaction ($S_{nl} = -\partial\Gamma_E/\partial f$). *Resio et al.* [2001] indicated that the net nonlinear energy flux has a cubic dependence on the normalized energy density Φ in the equilibrium range, and RLV04 presented the following relations:

$$\Gamma_E(f) - \Gamma_E(f_{eq}) \sim \int_{f_{eq}}^f \frac{\partial\Phi^3}{\partial f} df \sim \int_{f_{eq}}^f S_f df, \quad (4)$$

where f is an arbitrary frequency inside the equilibrium region and f_{eq} is the lower bound frequency for the equilibrium region. Equation (4) clearly demonstrates that any net gain or loss of wave energy within the equilibrium range would tend to force the spectrum away from an f^{-4} shape. If the net effect of S_f is negligible ($S_f \sim 0$) within the equilibrium range, the flux of energy due to nonlinear transfer Γ_E and saturation spectrum Φ should be constant; that is, $\Gamma_E(f) = \Gamma_E(f_{eq}) = \text{constant}$, and $\Phi^3(f) = \Phi^3(f_{eq}) = \text{constant}$. Because the frequency spectral tails measured in many field observations have exhibited the f^{-4} spectral form [e.g., *Donelan et al.*, 1985], the absolute value of the net external force S_f should

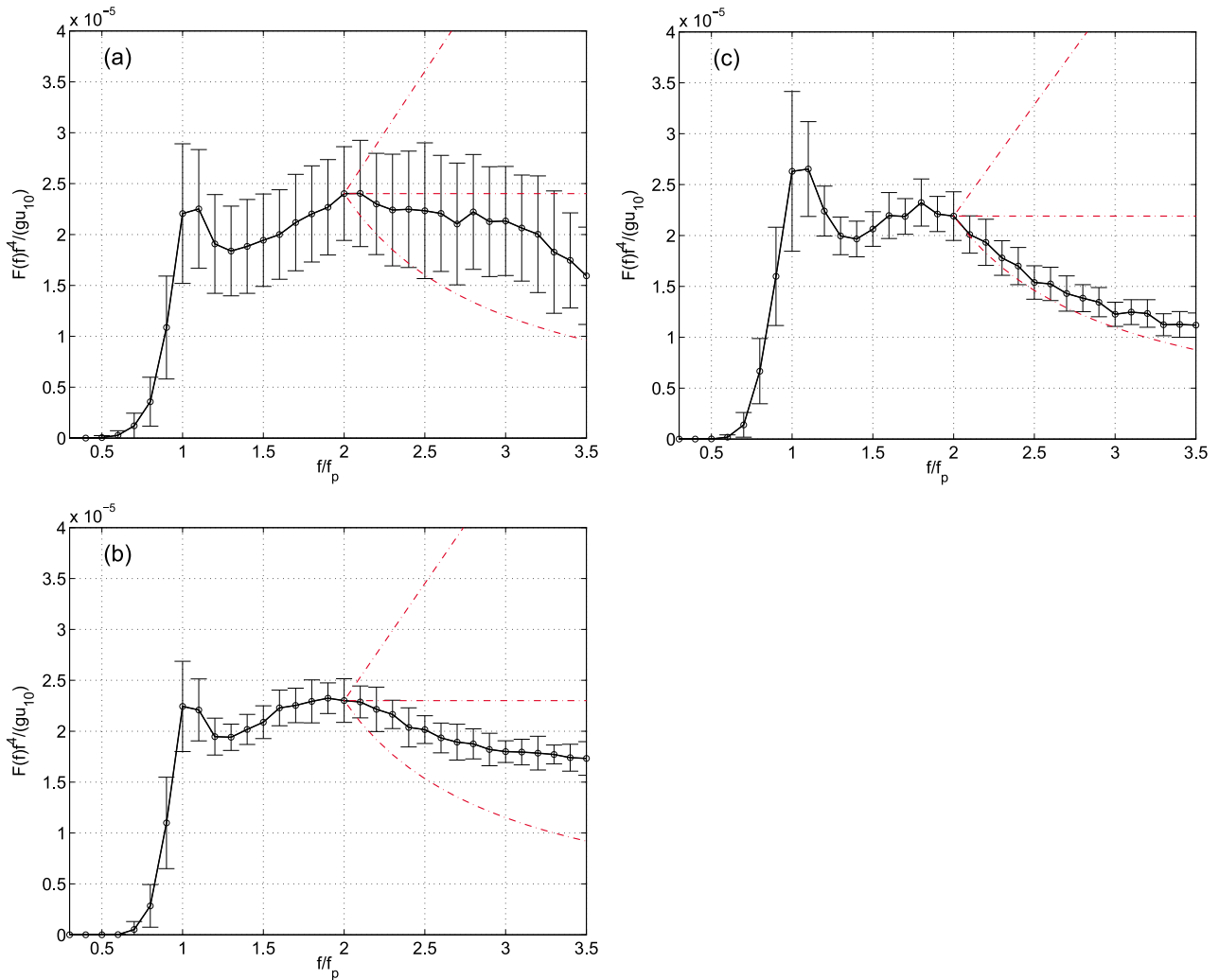


Figure 10. Mean and standard deviation of wave spectra at buoy 46006 for (a) NDBC observations, (b) calculation by SRIAM and (c) by DIA as the S_{nl} schemes. To investigate the higher-frequency part of the spectra, wave spectra were normalized in the form of equation (2). Red dashed/dotted lines represent the f^{-3} , f^{-4} , and f^{-5} power laws originating at $f/f_p=2$.

be negligible and thus the small imbalance between wind input and energy dissipation might be an important factor controlling the spectral shape in the equilibrium range.

[41] Before turning to the source balance in the equilibrium region, let us consider the source balance around the spectral peak region. Figure 11 presents the mean of the source functions of all spectra selected according to the same condition ($u_{10}/c_p > 1$) as in Figure 10. In the following analysis, each source term is normalized such that $S^* = S \cdot g^2 u_*^4$, where u_* is the friction velocity. Positive and negative peaks of S_{nl} appear around the spectral peak. In this region, the total source is dominated by S_{nl} with positive S_f . The total source term also shows transition of its peak value from positive to negative around the frequency peak, which resembles the S_{nl} shape. The wave spectrum grows rapidly on the forward face, whereas it attenuates on the rear face under the influence of the total source. These positive and negative energy inputs induce the overshoot and undershoot phenomena around the spectral peak [Holthuijsen, 2007].

[42] The difference in model performance between SRIAM and DIA can be explained by the shape of S_{nl} and the associated total source. As shown in Figure 11a, the transition from positive and negative sources is distributed in a narrow frequency band for SRIAM but is relatively broadly distributed for DIA. DIA treats one resonant configuration of four specific waves, which is rather wide in wave number space, to resolve the effects of S_{nl} in the peak [Van Vledder et al., 2000]. Therefore, its applicability to the narrow frequency spectrum is limited. On the other hand, SRIAM, which treats 20 resonant configurations, has sufficient flexibility to represent both broad and narrow spectral shapes and can capture realistic spectral shapes.

[43] In this hindcast experiment, the equilibrium spectrum appears for frequencies greater than 2.2–2.3 f_p where source terms cancel each other out and the total source term approaches zero. In this region, S_{nl} is smaller than the other sources, while the other two source terms are almost of the same order of magnitude. The net external source S_f is negative and balanced with positive S_{nl} in this region. As sug-

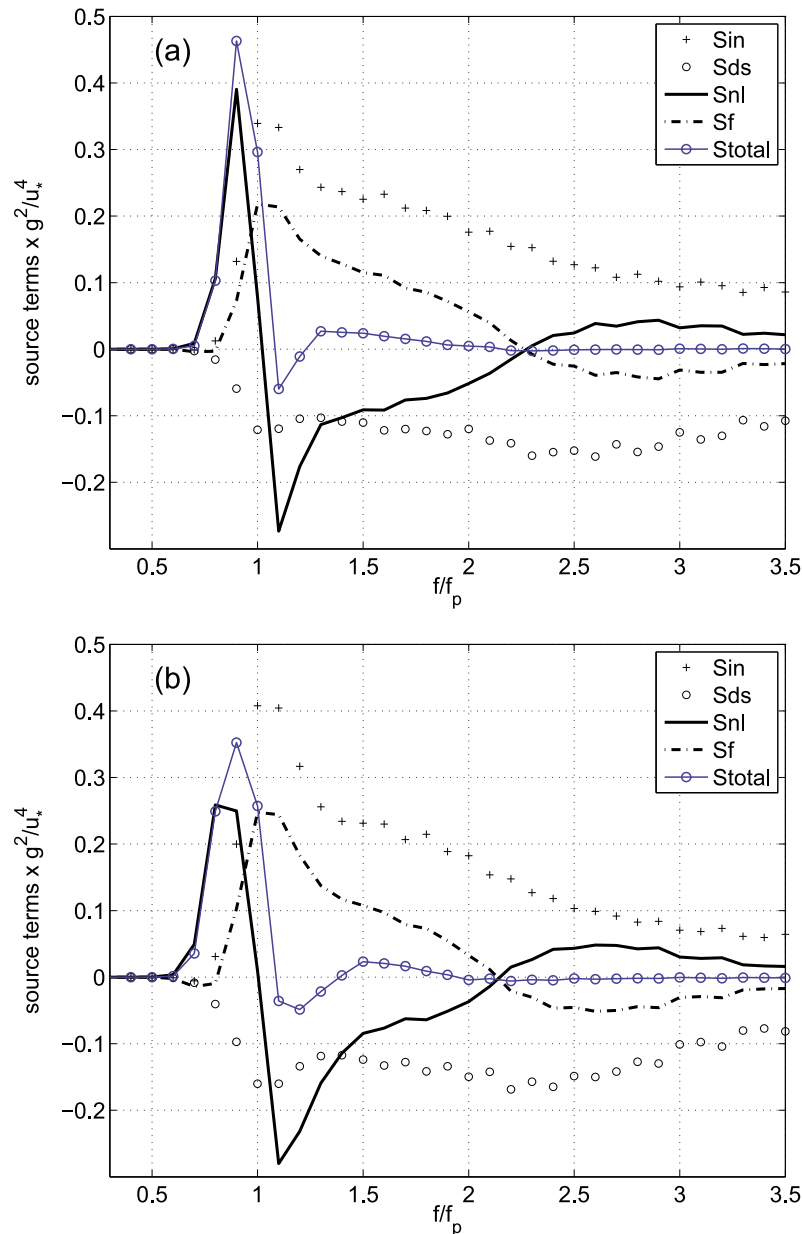


Figure 11. The mean of the source functions of all spectra calculated for the same condition (Figure 10) with (a) SRIAM and (b) DIA as the S_{nl} schemes. Each source term is normalized such that $S^* = S \cdot g^2 u_*^{-4}$.

gested by RLV04, the saturation spectrum falls off much more steeply than f^{-4} (see Figures 10b and 10c) because the net flux of wave energy due to S_{nl} is not constant in this hindcast experiment. In other words, the spectral tails calculated by both SRIAM and DIA do not follow the f^{-4} power law; they approach an exponent much smaller than -4 because of the negative S_f . Therefore, in numerical wave prediction, while the accuracy of the S_{nl} term is an important factor for confirming the constant flux of wave energy, S_f also has a major impact on the spectral shape in the equilibrium range.

[44] As indicated above, the spectral tail in the high-frequency region diverges from the f^{-4} shape. However, the model results still produce the equilibrium range during the wave growth in frequency ranges in which the total source term

tends to be zero. Therefore, to investigate which mechanism maintains the equilibrium range and the associated spectral shapes when the different source balance is imposed in the hindcast experiment, we conducted additional numerical experiments assuming different source balances. The high-frequency S_{ds} term was adjusted by multiplying the coefficient β ($=0, 0.25, 0.5, 0.6, 0.75$) as follows:

$$S_{total} = S_{in} + S_{nl}^{SRIAM} + \alpha \cdot (S_{ds}^{low} + \beta \cdot S_{ds}^{high}), \quad (5)$$

where $\alpha = 0.8$, and S_{ds}^{low} and S_{ds}^{high} represent the low- and high-frequency dissipation terms, respectively, defined by TC96.

[45] Figures 12a and 12b indicate the mean source balance for a growing windsea calculated for $\beta = 0$ and 0.6 , respec-

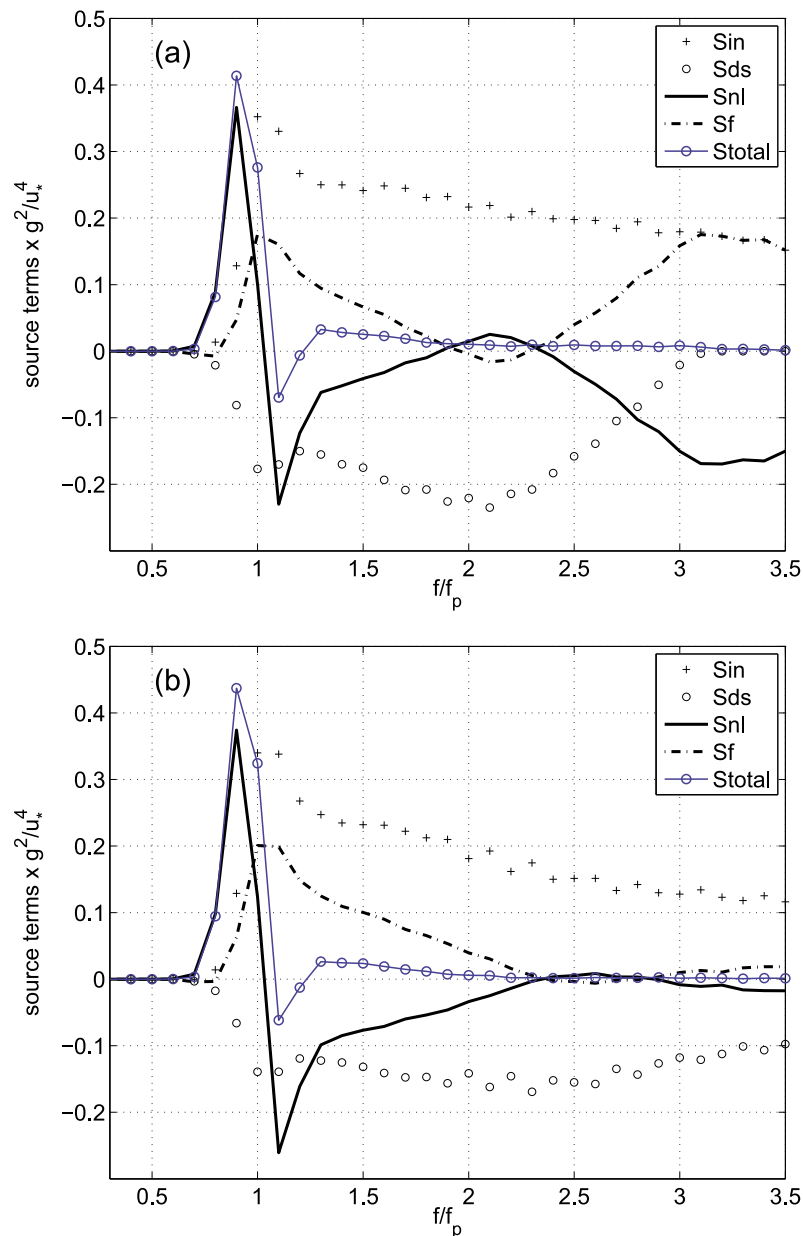


Figure 12. Same as Figure 11, but for other source balances with SRIAM: (a) high-frequency dissipation is completely neglected ($\beta = 0$), and (b) high-frequency dissipation is reduced by 40% ($\beta = 0.6$) from the original computation (Figure 11a).

tively. In the case of $\beta = 0$ (Figure 12a), the source balance in the high-frequency region is completely different from that in the previous hindcast (Figure 11a). Because the high-frequency dissipation term was set to zero in this experiment, total dissipation ($S_{ds}^{low} + S_{ds}^{high}$) gradually approaches zero from about $2f_p$ to $3f_p$, and the net external source S_f becomes positive in the high-frequency region ($f/f_p > 2.5$). Corresponding to the modulation of the S_{ds} term, the shape and magnitude of the S_{nl} term changes considerably such that the total source tends to be zero. At the same time, the mean spectral shape (not shown here) calculated by these source terms takes quite a different form from the previous result (Figure 10b); the spectral tail tends to be large and approaches an f^{-3} spectral shape. On the other hand, in the case of $\beta = 0.6$, S_f and S_{nl}

approach zero from about $2.3f_p$, and the spectral shape tends to follow an f^{-4} form.

[46] To confirm the relationship between the source term balance and the spectral shape more clearly, we compared the intensities of S_f and nonlinear transfer S_{nl} for all cases ($\beta = 0, 0.25, 0.5, 0.6, 0.75, \text{ and } 1$) as shown in the scatterplot in Figure 13. Each label was categorized according to β and corresponded to the instantaneous intensities of S_f and S_{nl} when inverse wave age u_{10}/c_p was greater than 1. Normalized source terms were integrated for $2.5\text{--}3.5 f/f_p$ to define the intensity of each source term. The results clearly demonstrate that the nonlinear transfer is in balance with S_f to cancel out the total source term; this means that the equilibrium range is controlled by the S_{nl} term whenever the three source terms are

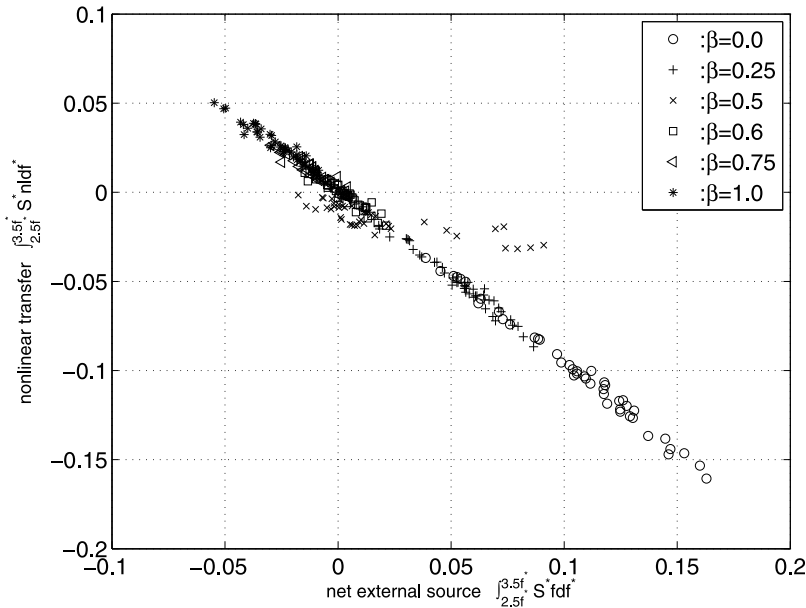


Figure 13. Scatterplot of the external source S_f and nonlinear transfer S_{nl} for all additional experiments (\circ : $\beta=0$, $+$: $\beta=0.25$, \times : $\beta=0.5$, \square : $\beta=0.6$, \triangleleft : $\beta=0.75$, $*$: $\beta=1.0$). Source terms are adopted instantaneously when the inverse wave age is greater than 1. Normalized source terms are integrated from $2.5 f/f_p$ to $3.5 f/f_p$ to define the intensity of each source term.

unbalanced in a growing windsea. In addition, the source terms of S_f and S_{nl} are plotted as instantaneous intensity (Figure 13). Hence S_{nl} reacts quickly to changes in the source balance.

[47] At the same time, the estimated exponent of the wave spectral tail varied from about -4.8 to -3.2 and was associated with S_f , as shown in Figure 14. When S_f was positive, the exponent was greater than -4 , whereas when S_f was negative, the exponent was less than -4 . These results completely

support the finding by RLV04 that any net gain or loss of wave energy within the equilibrium range would tend to force the spectrum away from an f^{-4} shape.

5. Summary and Discussion

[48] We investigated the impact of S_{nl} on wave fields by performing hindcast experiments for the Pacific Ocean. In particular, we evaluated model performance using SRIAM,

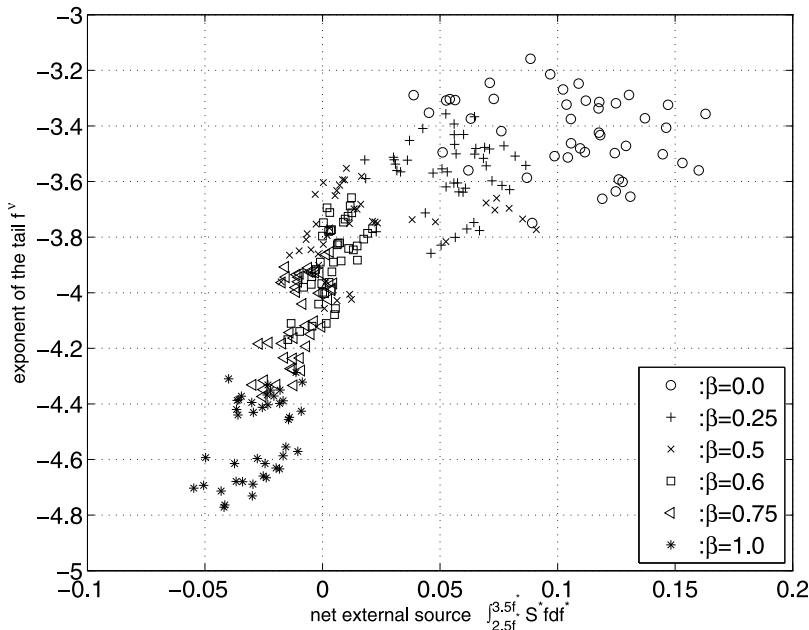


Figure 14. Intensity of the external source term versus the estimated exponent of the wave spectral tail. Symbols are the same as in Figure 13.

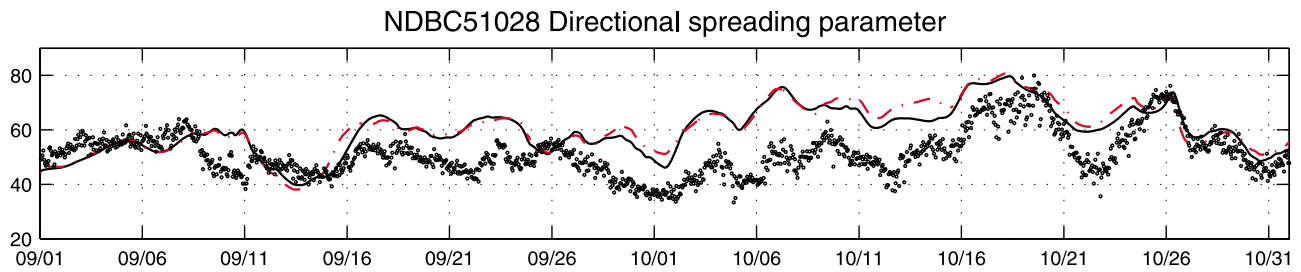


Figure 15. Time series of mean directional spreading σ_θ : circles represent in situ data, the solid black line is the computational result by SRIAM, and the red dashed/dotted line depicts the DIA result.

which was developed for operational use to accurately reproduce S_{nl} with lower computational costs compared to rigorous algorithms. This was assessed by comparing the model results to in situ wave parameters, as well as the results of another model run with the widely used DIA method. The results revealed that the difference in SRIAM and DIA performance depended on the time, location, and estimated wave parameters. In particular, the results using the two schemes differed quite prominently in their peak frequencies. The model performance of WW3 using SRIAM was improved around the tropical Pacific, characterized by mixed sea influenced by tradewinds and swells from higher latitudes. In addition, detailed analysis of the spectral shape revealed that SRIAM quantitatively captured the overshoot and undershoot phenomena around the spectral peak during wave growth. The S_{nl} term is important for maintaining the equilibrium range and crucial, along with the S_r term, for reproducing the f^{-4} power law behavior in the equilibrium range.

[49] Scatterplots (Figure 2b) and pdfs (Figure 4) of peak frequency and wave spectra (Figures 5 and 7) indicate that the f_p calculated using SRIAM was shifted to lower frequency. This improved the high-frequency bias of the spectral peak estimate with respect to DIA. Rogers *et al.* [2005] stressed that WW3 has a tendency to significantly (over-) underestimate wave energies at (high) low frequencies. It has not been mentioned directly, but previous studies have also indicated this kind of positive (negative) bias for the f_p (peak period) using DIA for the S_{nl} term (i.e., the original WW3). For example, Chao *et al.* [2005] conducted hindcasts of hurricane-induced waves using North Pacific hurricane (NPH) and western North Atlantic (WNA) wave models whose source terms consisted of the TC96 and DIA. Validation for the peak period indicated high CC (more than 0.7), but the biases of both models were negative for all locations (see Chao *et al.* [2005], their Table 2). Padilla-Hernández *et al.* [2007] also conducted hindcasts of storm-induced waves. The statistics for T_p calculated by default WW3 (TC96 and DIA) again indicated a negative bias for the peak period, as shown in Tables 3 and 4 of their paper. Our study shows that one of the main advantages of SRIAM is the reduction of the persistent bias of WW3 using DIA for f_p or the peak period. This should be important from a modeling viewpoint using third-generation models.

[50] We focused mainly on the wave parameters in the frequency domain, such as the Q_p parameter and the frequency spectrum. If good directional wave spectral measurements from an open ocean are available, we can evaluate and calibrate the wave model. Then the source terms can be tuned to fit observations with regard to directionality. The S_{in} and S_{ds}

terms should be corrected and calibrated against observations using an accurate S_{nl} term, which would lead to improved wave modeling. However, it is not easy to assess model performance for the directional spectrum and the associated directional spreading because the observational data needed for such validation are still limited spatially. Furthermore, the available data, such as historical data from NDBC buoys, include only estimates of the lower-order (first and second pair) Fourier coefficients of the directional spreading function; higher-order Fourier components are neglected. Because of these problems and limitations, we cannot discuss with confidence the model performance with regard to wave directionality, such as the normalized directional distribution “A” proposed by Babanin and Soloviev [1998]. An example of the time series of the mean directional spreading σ_θ [Kuik *et al.*, 1988] at 51028 (the equatorial Pacific) is given in Figure 15, where σ_θ is defined as follows:

$$\bar{\sigma}_\theta = 180\pi^{-1} \left[2 \left(1 - \sqrt{(a_1^2 + b_1^2) \cdot m_0^{-1}} \right) \right]^{0.5}, \quad (6)$$

where θ is the wave direction and components of the mean wave direction a_1 and b_1 are defined as the first pair of Fourier coefficients:

$$a_1 = \int_0^{2\pi} \int_0^\infty \cos(\theta) F(f, \theta) df d\theta, \quad b_1 = \int_0^{2\pi} \int_0^\infty \sin(\theta) F(f, \theta) df d\theta. \quad (7)$$

[51] σ_θ values estimated by the wave models clearly have a positive bias, as shown in Figure 15. This might be due to the artificial background swells, which were also confirmed for the wave peakedness parameter Q_p in the lower-latitude Pacific (51004), as shown in Figure 9. Whereas the model bias of σ_θ was evident, it is encouraging that both model results seem to provide a reasonable representation of the time variations. In addition, the σ_θ values attained by DIA were usually somewhat larger than those by SRIAM, which is consistent with model results, as shown in the previous sections. Tamura *et al.* [2009] conducted a hindcast simulation to reproduce the sea state at the time of a shipwreck possibly induced by an encounter with abnormal waves. Hindcast results indicated that while the absolute value of σ_θ was insufficient to produce the quasi-resonance that causes freak waves, the time history of the hindcast result clearly indicated a decreasing trend in the wave directionality at the time of the incident. To improve freak wave prediction, we must know how well models can

estimate directional spreading, and the estimated parameters need to be calibrated against observations.

[52] Regarding the equilibrium condition, in many studies [e.g., *Komen et al.*, 1984; *Phillips*, 1985; TC96] the total source terms were considered to be zero to maintain the equilibrium region of the wave spectrum; i.e., as given in equation (3). Then the shape of the source terms S_{in} and S_{ds} are assumed to balance each other and to satisfy the necessary condition as also indicated in equation (3). In particular, the S_{ds} term is often considered the “tuning knob” in the wave model, derived as the residual of the unknown term in equation (3). However, the present study indicates a different formation process of the source balance in the equilibrium range. The total source term approached zero during wave evolution, regardless of which S_f function was used. S_{nl} plays a major role in the adjustment of the total source balance. Our results demonstrate that the balance of the equilibrium condition (3) is maintained by the S_{nl} term.

[53] Previous works have investigated the role of source terms and their balance in a growing windsea. *Kitaigorodskii* [1983] derived an f^{-4} spectral tail based on the assumption that the energy flux due to S_{nl} is constant inside the equilibrium range and that source terms are negligible ($S_{in} \sim S_{nl} \sim S_{ds} \sim 0$) to maintain it. On the other hand, *Phillips* [1985] investigated the relative roles of the source terms and concluded that all three are of the same order of magnitude ($S_{in} \sim S_{nl} \sim S_{ds}$) in representing the f^{-4} spectral tail. *Banner and Young* [1994] investigated the influence of the level of dissipation and demonstrated that the magnitude of S_{ds} influences the amount of energy in the spectral tail but has little influence on the decay exponent. *Young and Van Vledder* [1993] also stated that the energy level in the spectral tail is sensitive to the choice of S_{in} and S_{ds} ; however, the exponent of the spectral tail is less sensitive. The present study also demonstrates that the sum of the three source terms approaches zero largely as a result of S_{nl} adjustment. However, the exponent of the spectral tail was also quite sensitive to S_f in agreement with RLV04. SRIAM can reproduce the time evolution of the spectral shape to formulate the f^{-4} tail when the kinetic equation is simply integrated in time (not shown here). This suggests that SRIAM can also force the spectral tail to take an f^{-4} form, as in an exact S_{nl} computation [e.g., *Resio et al.*, 2001]. However, the net external source S_f is the key factor that reproduces the f^{-4} tail, and “ $S_f \sim 0$ inside the equilibrium range” might be considered a constraint in numerical wave modeling to guarantee the -4 exponent.

[54] **Acknowledgments.** We are grateful to two reviewers for their careful reading of this paper and their constructive comments, which were very helpful in improving the manuscript. This work is part of the Japan Coastal Ocean Predictability Experiment (JCOPE) supported by the Japan Agency for Marine–Earth Science and Technology. Takuji Waseda was also supported by a Grant-in-Aid for Scientific Research from the Japan Society for the Promotion of Science.

References

- Ardhuin, F., T. H. C. Herbers, G. P. Van Vledder, K. P. Watts, R. Jensen, and H. C. Graber (2007), Swell and slanting fetch effects on wind wave growth, *J. Phys. Oceanogr.*, *37*, 908–931.
- Babanin, A. V., and Y. P. Soloviev (1998), Variability of directional spectra of wind-generated waves, studied by means of wave staff arrays, *Mar. Freshwater Res.*, *49*, 89–101.
- Badulin, S. I., A. N. Pushkarev, D. Resio, and V. E. Zakharov (2005), Self-similarity of wind-driven seas, *Nonlin. Proc. Geophys.*, *12*, 891–945.
- Banner, M. L., and I. R. Young (1994), Modeling spectral dissipation in the evolution of wind waves. Part I: Assessment of existing model performance, *J. Phys. Oceanogr.*, *24*, 1550–1571.
- Barnett, T. P., and J. C. Wilkerson (1967), On the generation of ocean wind waves as inferred from airborne radar measurements of fetch-limited spectra, *J. Mar. Res.*, *25*, 292–321.
- Bidlot, J., et al. (2007), Inter-comparison of operational wave forecasting systems, 10th International Workshop on Wave Hindcasting and Forecasting and Coastal Hazard Symposium, North Shore, Oahu, Hawaii.
- Cardone, V. J., R. E. Jensen, D. T. Resio, V. R. Swail, and A. T. Cox (1996), Evaluation of contemporary ocean wave models in rare extreme events: The “Halloween Storm” of October 1991 and the “Storm of the Century” of March 1993, *J. Atmos. Oceanic Technol.*, *13*, 198–230.
- Chao, Y. Y., J. H. G. M. Alves, and H. L. Tolman (2005), An operational system for predicting hurricane-generated wind waves in the North Atlantic Ocean, *Weather Forecasting*, *20*(4), 652–671.
- Donelan, M. A., J. Hamilton, and W. H. Hui (1985), Directional spectra of wind-generated waves, *Philos. Trans. R. Soc. London A*, *315*, 509–562.
- Goda, Y. (2000), *Random Seas and Design of Maritime Structures*, *Adv. Ser. Ocean Eng.*, vol. 15, 443 pp., Univ. of Tokyo Press, Tokyo, Japan.
- Gramstad, O., and K. Trulsen (2007), Influence of crest and group length on the occurrence of freak waves, *J. Fluid Mech.*, *582*, 463–472.
- Hansen, C., K. B. Katsaros, S. A. Kitaigorodskii, and S. E. Larsen (1990), The dissipation range of wind-wave spectra observed on a lake, *J. Phys. Oceanogr.*, *20*, 1264–1277.
- Hasselmann, K. (1962), On the nonlinear energy transfer in a gravity-wave spectrum I. General theory, *J. Fluid Mech.*, *12*, 481–500.
- Hasselmann, K., et al. (1973), Measurements of wind wave growth and swell decay during the Joint North Sea Wave Project (JONSWAP), *Dt. Hydrogr. Z.*, *A8*(12), 95 pp.
- Hasselmann, S., K. Hasselmann, J. H. Allender, and T. P. Barnett (1985), Computations and parameterizations of the nonlinear energy transfer in a gravity-wave spectrum. Part II: Parameterizations of the nonlinear energy transfer for application in wave models, *J. Phys. Oceanogr.*, *15*, 1378–1391.
- Holthuijsen, L. H. (2007), *Waves in Oceanic and Coastal Waters*, Cambridge Univ. Press, Cambridge, U. K., 387 pp.
- Janssen, P. A. E. M. (2003), Nonlinear four-wave interactions and freak waves, *J. Phys. Oceanogr.*, *33*, 863–884.
- Janssen, P. A. E. M., and J. Bidlot (2003), New wave parameters to characterize freak wave conditions. Research Dept. Memo. R60.9.PJ/0387, ECMWF, Reading, U. K.
- Kahma, K. K., and C. J. Calkoen (1994), Growth curve observations, in *Dynamics and Modelling of Ocean Waves*, edited by G. J. Komen et al., Cambridge Univ. Press, Cambridge, U. K., 174–182.
- Kalnay, E., et al. (1996), The NCEP/NCAR 40-year reanalysis project, *Bull. Amer. Meteor. Soc.*, *77*, 437–471.
- Kitaigorodskii, S. A. (1983), On the theory of the equilibrium range in the spectrum of wind-generated gravity waves, *J. Phys. Oceanogr.*, *13*, 816–827.
- Komatsu, K. (1996), Development of a new generation wave forecasting model based on a new scheme of nonlinear energy transfer among wind waves. Ph.D. thesis, Kyushu University, Japan, 155 pp. (in Japanese) (unpublished).
- Komatsu, K., and A. Masuda (1996), A new scheme of nonlinear energy transfer among wind waves: RIAM method. Algorithm and performance, *J. Oceanogr.*, *52*, 509–537.
- Komen, G. J., K. Hasselmann, and K. Hasselmann (1984), On the existence of a fully developed wind-sea spectrum, *J. Phys. Oceanogr.*, *14*(8), 1271–1285.
- Komen, G. J., L. Cavaleri, M. Donelan, K. Hasselmann, S. Hasselmann, and P. A. E. M. Janssen (1994), *Dynamics and Modelling of Ocean Waves*, Cambridge Univ. Press, Cambridge, U. K., 532 pp.
- Kuik, A. J., G. P. van Vledder, and L. H. Holthuijsen (1988), A method for the routine analysis of pitch-and-roll buoy wave data, *J. Phys. Oceanogr.*, *18*, 1020–1034.
- Long, C. E., and D. T. Resio (2007), Wind wave spectral observations in Currituck Sound, North Carolina, *J. Geophys. Res.*, *112*, C05001, doi:10.1029/2006JC003835.
- Mitsuyasu, H. (1968), On the growth of the spectrum of wind generated waves, I. *Rept. Res. Inst. Appl. Mech., Kyushu Univ.*, *16*, 459–465.
- Mitsuyasu, H. (1969), On the growth of the spectrum of wind generated waves, II. *Rept. Res. Inst. Appl. Mech., Kyushu Univ.*, *17*, 235–243.
- Onorato, M., A. R. Osborne, and M. Serio (2002), Extreme wave events in directional, random oceanic sea states, *Phys. Fluids*, *14*(4), 25–28.
- Padilla-Hernández, R., W. Perrie, B. Toulany, and P. C. Smith (2007), Modeling of two Northwest Atlantic Storms with third-generation wave models, *Weather Forecasting*, *22*(6), 1229–1242.
- Phillips, O. M. (1985), Spectral and statistical properties of the equilibrium range of wind-generated gravity waves, *J. Fluid Mech.*, *156*, 505–531.

- Pushkarev, D., T. Resio, and V. E. Zakharov (2003), Weak turbulent approach to the wind-generated gravity sea waves, *Physica D-Nonlinear Phenomena*, *184*, 29–63.
- Resio, D. T., and W. Perrie (1991), A numerical study of nonlinear energy fluxes due to wave-wave interactions. Part I: Methodology and basic results, *J. Fluid Mech.*, *223*, 609–629.
- Resio, D. T., and W. Perrie (2008), A two-scale approximation for efficient representation of nonlinear energy transfers in a wind wave spectrum. Part I: Theoretical development, *J. Phys. Oceanogr.*, *38*, 2801–2816, doi:10.1175/2008JPO3713.1.
- Resio, D. T., J. H. Pihl, B. A. Tracy, and C. L. Vincent (2001), Nonlinear energy fluxes and the finite depth equilibrium range in wave spectra, *J. Geophys. Res.*, *106*(C4), 6985–7000, doi:10.1029/2000JC900153.
- Resio, D. T., C. E. Long, and C. L. Vincent (2004), Equilibrium-range constant in wind-generated wave spectra, *J. Geophys. Res.*, *109*, C01018, doi:10.1029/2003JC001788.
- Rogers, W. E., P. A. Wittmann, D. W. C. Wang, R. M. Clancy, and Y. L. Hsu (2005), Evaluations of global wave prediction at the Fleet Numerical Meteorology and Oceanography Center, *Weather Forecasting*, *20*, 745–760.
- Tamura, H., T. Waseda, Y. Miyazawa, and K. Komatsu (2008), Current-induced modulation of the ocean wave spectrum and the role of nonlinear energy transfer, *J. Phys. Oceanogr.*, *38*, 2662–2684, doi:10.1175/2008JPO4000.1.
- Tamura, H., T. Waseda, and Y. Miyazawa (2009), Freakish sea state and swell-windsea coupling: Numerical study of the Suwa-Marui incident, *Geophys. Res. Lett.*, *36*, L01607, doi:10.1029/2008GL036280.
- Toba, Y. (1973), Local balance in the air-sea boundary processes III. On the spectrum of wind waves, *J. Oceanogr. Soc. Japan*, *29*, 209–220.
- Tolman, H. L. (2002), User manual and system documentation of WAVE-WATCH-III version 2.22. Tech. Note, 222, NOAA/NWS/NCEP/MMAB, 133 pp.
- Tolman, H. L. (2003), Treatment of unresolved islands and ice in wind wave models, *Ocean Modelling*, *5*, 219–231.
- Tolman, H. L. (2004), Inverse modeling of discrete interaction approximations for nonlinear interactions in wind waves, *Ocean Modelling*, *6*, 405–422.
- Tolman, H. L., and D. V. Chalikov (1996), Source terms in a third-generation wind wave model, *J. Phys. Oceanogr.*, *26*, 2497–2518.
- Tolman, H. L., V. M. Krasnopolsky, and D. V. Chalikov (2005), Neural network approximations for nonlinear interactions in wind wave spectra: Direct mapping for wind seas in deep water, *Ocean Modelling*, *8*, 253–278.
- Van Vledder, G. P. (2001), Extension of the discrete interaction approximation for computing nonlinear quadruplet wave-wave interactions in operational wave prediction models, 4th International Symposium on Ocean Waves, Measurement & Analysis, San Francisco, Calif.
- Van Vledder, G. P. (2006a), The WRT method for the computation of non-linear four-wave interactions in discrete spectral wave models, *Coastal Eng.*, *53*, 223–242.
- Van Vledder, G. P. (2006b), Towards an optimal computation of non-linear four-wave interactions in operational wave models, 9th Int. Workshop on Wave Hindcasting and Forecasting, Victoria, BC, Canada.
- Van Vledder, G. P., and J. A. Battjes (1992), Discussion on list of sea state parameters, *ASCE J. Port. Harbor Ocean Eng.*, *118*, 226–228.
- Van Vledder, G. P., T. H. C. Herbers, R. E. Jensen, D. T. Resio, and B. Tracy (2000), Modeling of non-linear quadruplet wave-wave interactions in operational wave models. Proc. 27th Int. Conf. on Coastal Engineering, Sydney, Australia.
- Wang, W., and R. X. Huang (2004), Wind energy input to the surface waves, *J. Phys. Oceanogr.*, *34*, 1276–1280.
- Waseda, T., T. Kinoshita, and H. Tamura (2009a), Evolution of a random directional wave and freak wave occurrence, *J. Phys. Oceanogr.*, *38*, 621–639.
- Waseda, T., T. Kinoshita, and H. Tamura (2009b), Interplay of resonant and quasi-resonant interaction of the directional ocean waves, *J. Phys. Oceanogr.*, *39*, 2351–2362.
- Xu, F., W. Perrie, B. Toulany, and P. C. Smith (2007), Wind-generated waves in Hurricane Juan, *Ocean Modelling*, *16*, 188–205.
- Young, I. R., and G. P. Van Vledder (1993), A review of the central role of nonlinear interactions in wind-wave evolution, *Trans. R. Soc. London*, *342*, 505–524.
- Zakharov, V. E., and N. N. Filonenko (1966), The energy spectrum for stochastic oscillation of a fluid's surface, *Dokl. Akad. Nauk.*, *170*, 1992–1995.

Y. Miyazawa, H. Tamura, and T. Waseda, Research Institute for Global Change, Japan Agency for Marine-Earth Science and Technology, Yokohama, Kanagawa, 236-0001, Japan. (htamura@jamstec.go.jp)